The principles behind Non-Photochemical Laser Induced Nucleation

Davey Pieter Aad Nijland

Technische Universiteit Delft

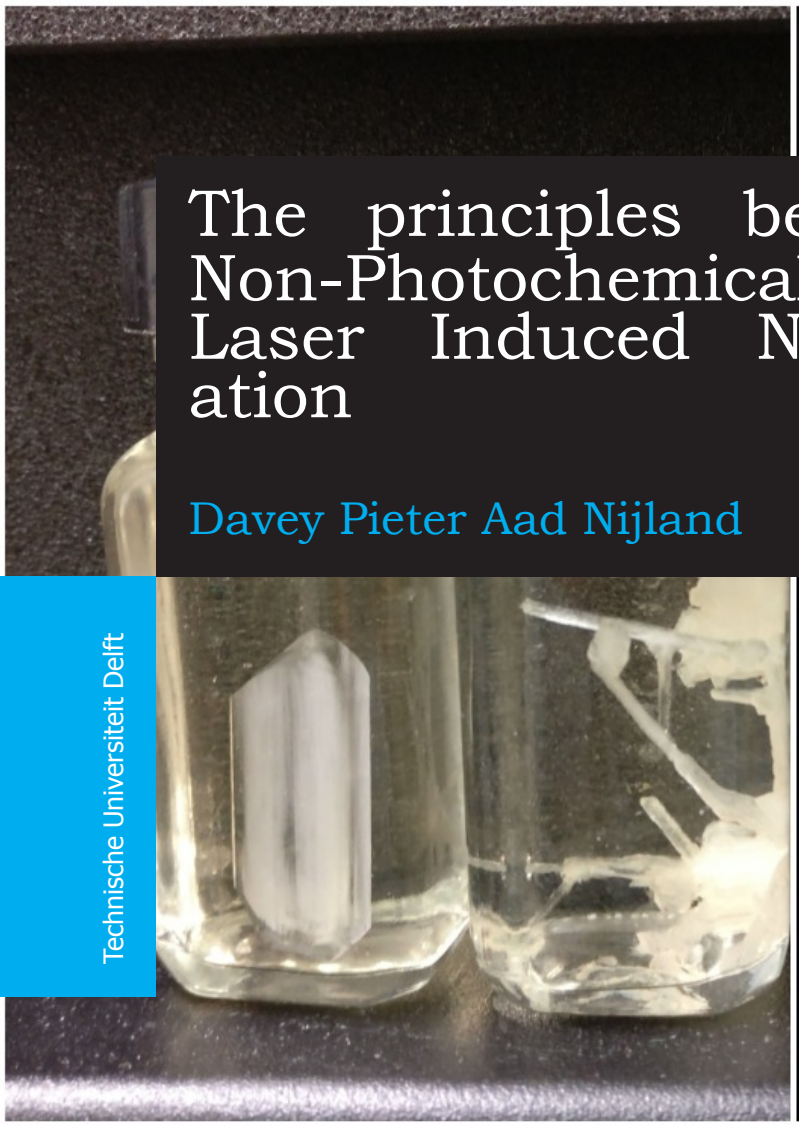

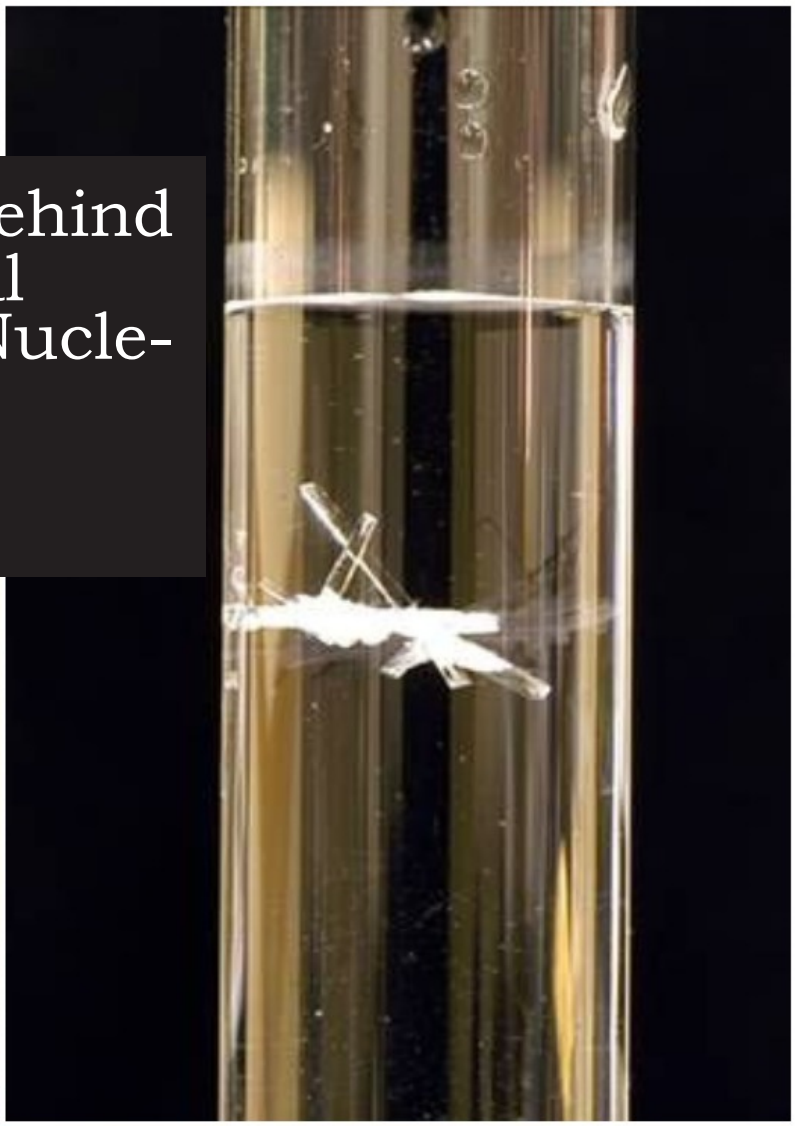

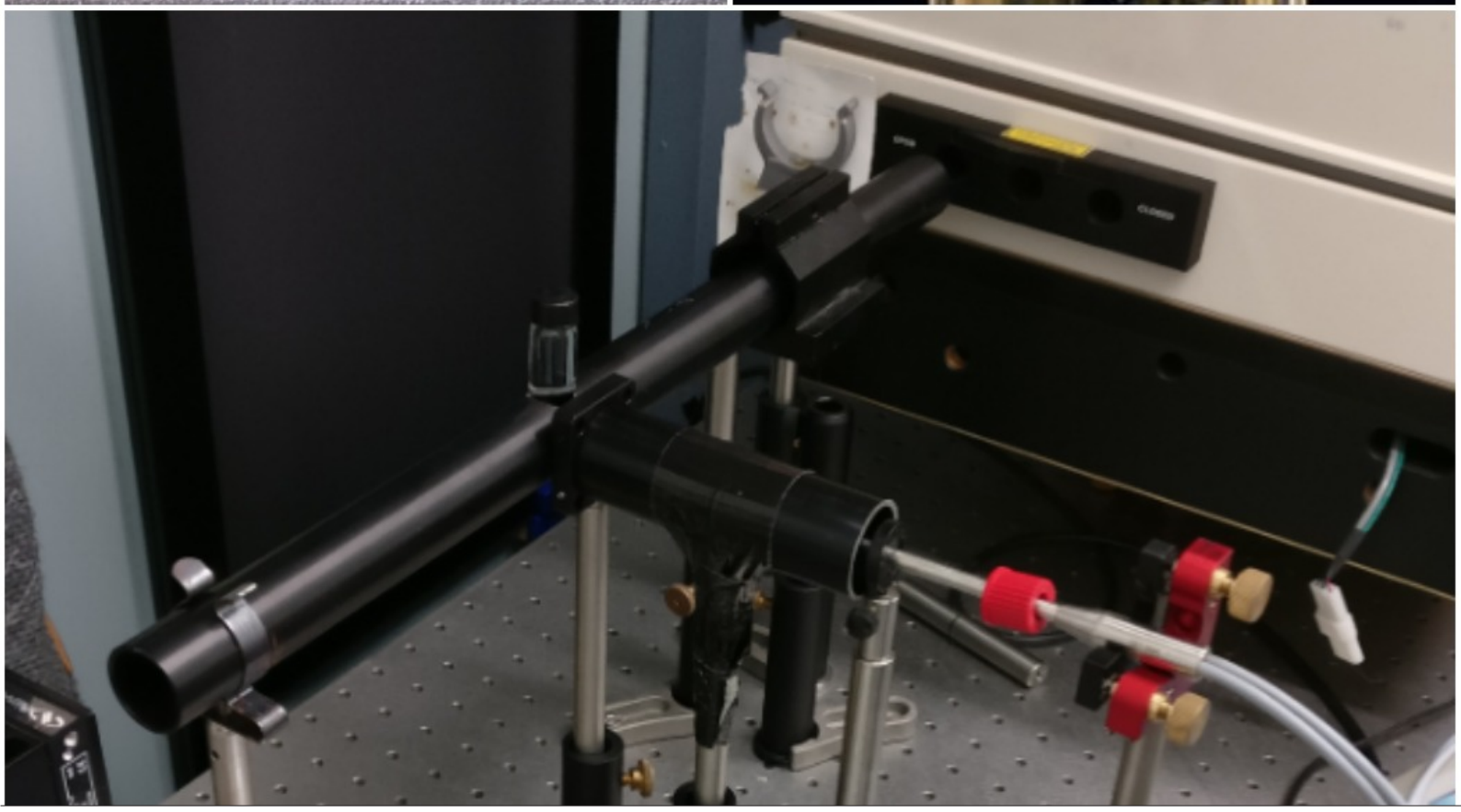

TU Delft Delft University of Technology

Challenge the future

The principles behind Non-Photochemical Laser Induced Nucleation

by

Davey Pieter Aad Nijland

in partial fulfillment of the requirements for the degree of

Master of Science
in Chemical Engineering

at the Delft University of Technology,
to be defended publicly on Thursday May 16, 2019 at 11:00 AM.

Report number:	P&E-2912	
Student number:	4600142	
Project duration:	September 1, 2018 – May 2, 2019	
Under guidance and supervision of:	Dr. H. B. Eral,	TU Delft
	Dr. D. Irimia,	TU Delft
	Dr. ir. H. J. M. Kramer,	TU Delft
	Prof. Dr. A. van der Heijden,	TU Delft
Thesis committee:	Dr. H. B. Eral,	TU Delft
	Prof. Dr. A. van der Heijden,	TU Delft
	Dr. M. A. van der Veen,	TU Delft

This thesis is confidential and cannot be made public until May 16, 2019.

TU Delft Delft University of Technology

Preface

I would like to express my gratitude to my supervisor Dr. Burak Eral and Dr. Daniel Irimia for their invaluable advice and guidance. Their expertise and patience really added to my graduate experience and this research. Daily discussions with Daniel kept me on the right track finding the most useful information to enhance future success of the NPLIN project.

Besides these wonderful men, a special thanks go out to Dr. Herman Kramer and Prof. Dr. Antoine van der Heijden, for their time, feedback and supervision during the NPLIN meetings. Their input enabled new insights, required a critical look at my own work and shed light on different perspectives.

Finally, I would like to thank my family and Shannon in particular. You supported me the whole adventure that is called my Chemical Engineering masters. Thank you for your patience, your advice and doing the household when I could not.

I don't have dreams, I have goals. Now it's on to the next one.

Davey Pieter Aad Nijland
Delft, April 2019

Abstract

Crystallization is a process known to humankind for centuries. Everyday items can be a result of crystallization, e.g. snowflakes being formed in cold weather and sugar that is obtained from glucose-water solutions. Crystallization follows from the process which is called nucleation. This phenomenon is explained in two different theories: classical nucleation theory and two-step nucleation theory. Also, two different ways of crystallization can be distinguished: heterogeneous nucleation, which is nucleation that evolves from external surfaces and homogeneous nucleation, which obviously evolves without the help of external surfaces.

Methods to perform crystallization, based on aforementioned mechanisms, are useful for production scale facilities as it is a very useful method to separate chemicals in manufacturing processes. However, large scale crystallization processes are known to be hard to control and energy intensive, something that does not fit into today's society. To keep up with the global demand for sustainable production novel crystallization methods need to be established. A promising finding, 20 years ago, consisted of laser-induced nucleation. By means of a laser, Garetz et al.[1] were able to induce crystallization, calling it non-photochemical laser induced nucleation (NPLIN). Up to this date, it is not known what mechanisms underlie the observed behavior. Because the phenomenon was only observed at the milliliter range, it is important to understand the mechanisms before further upscaling can be done. Over the course of the last decade, 4 mechanisms have been proposed: Optical Kerr effect, Isotropic electronic polarization, nano-impurities, and shockwaves.

During the discovery of NPLIN, it was found that the wavelengths and power intensity were incapable of creating a photochemical effect on the compound used. For this reason, the LIN was ascribed to non-photochemical behavior. In this research, more detail is provided on this presumed non-photochemical effect. An experimental build is established to perform multiple experiments for detecting radicals and obtain consensus on the attributed name. Initial tests revealed that there is no particular interaction between the solute and laser electric field.

Throughout the research, several factors were found to play a role in observed NPLIN behavior. Over the course of this project, glycine samples started to turn yellow due to the degradation of glycine. pH was found to be an important factor for polymorphic control, however, it was constant for all samples since glycine acted as a buffering agent. Future research with new chemicals should keep track of the pH together with polymorphism. Glass geometries tests showed that container curvatures are affecting the polarization of the laser and thus the outcomes for polymorphic structures.

At last, the effect of impurities on NPLIN was elaborated. Doping samples intentionally with nano-impurities resulted in higher crystallization probabilities. On the other hand, reducing the impurity levels also decreased the nucleation probability. It is concluded that impurities are highly correlated to nucleation performance. Moreover, the laser-interaction volume is also affecting the nucleation probability in significant amounts. Supplementary research is required to obtain a set of operating parameters that have an effect on NPLIN behavior. With such a model, NPLIN can be controlled and a state of the art production scale laser induced nucleation unit becomes the new standard.

Contents

List of Figures

1

Introduction

Crystallization is the natural phenomenon causing snowflakes to form from water, sugar crystals to sprout from honey and minerals to be created in rock formations. Although the phenomenon itself is known since time immemorial, it is still not completely understood what mechanisms account for the first steps, which makes it harder to fully control the process. Luckily, this does not hamper the use of novel crystallization techniques in all kind of human-made processes, where crystallization is used to purify the dissolved compound by changing it back into its solid state. These techniques include the use of cooling, crystallization and reactive crystallization with the assistance of, for instance, mechanic shocks, electric fields, ultrasound and magnetic fields [2–4]. This work elaborates on the use of lasers to enhance crystallization behavior, namely non-photochemical laser induced nucleation (NPLIN).

1.1. Crystallization

Crystallization is a process that can be described by two theories, classical nucleation theory and two-step nucleation theory. Both these theories provide sufficient evidence to explain parts of crystallization nature. However, at the same time, they are not accurate enough to describe all the observed phenomena. Two things that are known for sure are primary and secondary nucleation. These two types of nucleation are describing the ways how nucleation can be induced.

1.1.1. Classical Nucleation Theory and Two-Step Nucleation Theory

Up to this date, crystallization is believed to follow either a two-step model or the classical nucleation model. The classical nucleation theory is the oldest model and suggests that clusters of solute molecules are formed up to the point where they reach a certain critical size causing them to retain the characteristics of a solid particle on which the crystallization process continues. Two-step nucleation, on the other hand, assumes two consecutive steps consisting of large density fluctuations and the formation of a crystalline nucleus [5].

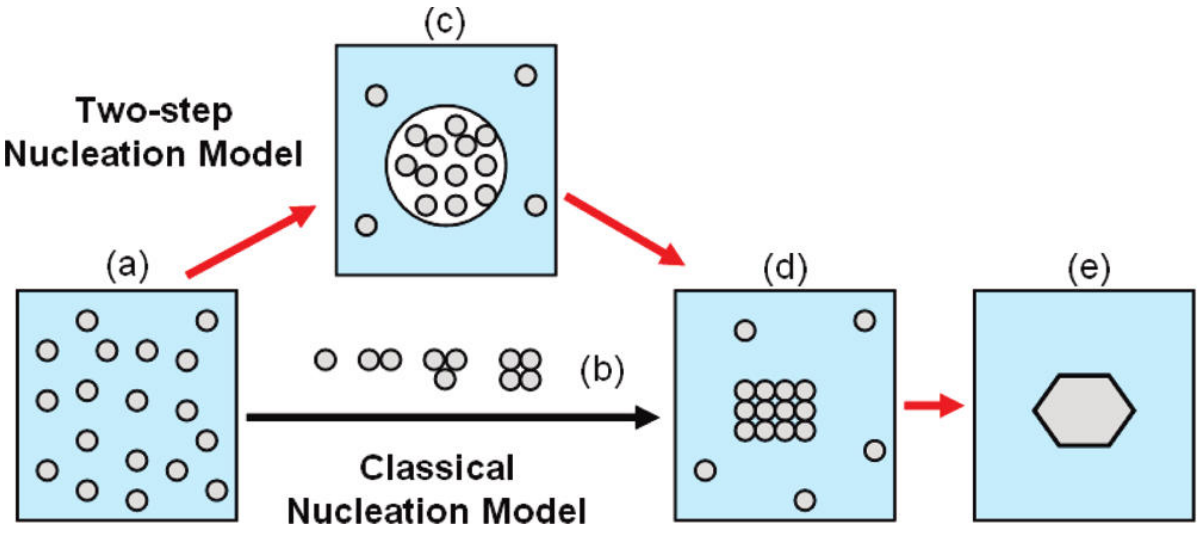

Figure 1.1: Both crystallization theories visualized [5]

As can be seen in figure 1.1 the two-step model is an addition to the already existing classical nucleation theory. In classical nucleation the dissolved species are moving around as shown in 1.1(a). Due to the random collisions inside the solution, small clusters are formed by solute molecules that stick together. Other molecules bump onto the cluster, enlarging its size 1.1(b). At the same time, molecules leave the cluster, 1.1(d), resulting in an equilibrium state between different cluster sizes. When the cluster reaches its critical size, a minor energy boost is enough to overcome its free Gibbs energy (δG) resulting in disequilibrium in the aforementioned system, making the cluster bigger and bigger until it becomes a stable crystal, 1.1(e).

In the two-step model, the cluster pathway is assumed to be more instantaneous. Large density fluctuations promote the formation of highly disordered liquid droplets as shown in 1.1(c). Within this high-density droplet, the formation of a crystalline nucleus with a certain critical size is obtained.

1.1.2. Primary and secondary crystallization

Next to the two proposed theories, the nucleation process is attributed to two mechanisms, primary and secondary nucleation [6]. Primary nucleation is divided into homogeneous and heterogeneous nucleation while secondary nucleation is a phenomenon itself.

Primary nucleation; Homogeneous nucleation is also known as spontaneous nucleation. This mechanism mainly refers to the theories mentioned in section 1.1.1. In spontaneous nucleation, no additional step is undertaken to promote nucleation. Making it a perfect explanation for the classical nucleation theory, where clusters are increasing in size randomly until they reach their critical size and start to crystallize.

Primary nucleation; Heterogeneous nucleation, on the other hand, is more susceptible to external fluctuations. It is characterized by the addition of foreign particles that promote nucleation by providing an external surface for the molecules to collide and settle. It is assumed that the molecules are more likely to stick to this external surface and thus the cluster formation is positively stimulated.

Secondary nucleation can be described by heterogeneous nucleation where crystals from the solute are added deliberately. This, so-called seeding, is a conventional way to produce larger crystals by simply adding seeding crystals into a supersaturated solution of that particular solute. The crystal starts to attract surrounding molecules enabling density fluctuations that enhance crystallization. Secondary nucleation will often favor the formation of a certain crystal shape, making it possible to control the polymorphism.

1.2. Polymorphism

Polymorphism is a well-known, yet not fully understood subject within the world of crystallization. A polymorph consists of the same atoms while maintaining a different crystalline structure. This difference in structure causes the material to have different chemical properties, such as melting point, solubility, and hardness [7]. Applications for polymorphism are mostly found in the pharmaceutical segment where a higher solubility for the same compound can enhance the dissolving abilities of medicine. Such applications rose the awareness and interests for polymorphism a lot over the last century [8].

Several techniques are proposed to enable control of the polymorph-formation during crystallization, one being more novel than the other. The most convenient ways of producing a polymorph are seeding or the addition of soluble additives that inhibit the growth of a preferred polymorph. Newer crystallization techniques such as employing microporous membranes and sonocrystallization are still in the infancy and need more time to be developed as a good alternative for seeding or using soluble additives [8]. Non-Photochemical laser induced nucleation (NPLIN) has also proven to be a promising method for the formation of particular polymorphs. Sun et al. [9] were the first to discover a polarization switching window in which the polymorph of glycine was dependent on the concentration of solute and the polarization of the laser beam being used. Over time, other compounds including carbamazepine [10], L-histidine [11], and sulfathiazole [12], have found to be dependent on this polarization switching as well.

1.3. Laser induced nucleation

One way to form the solid phase from a solution is to perform laser induced nucleation (LIN). LIN is a method that requires a laser beam of a certain wavelength, depending on the internal bonds of a molecule, with a certain energy output to cause ionization or to create radicals that subsequently react to produce nucleation centers that promote nucleation [13]. However, in the various articles that have been published by the groups of Alexander [3, 12–20], Garetz [1, 2, 7, 9, 11, 21–24] and Eral [25–28], the power output used are orders of 10^4 lower than required to account for molecular bond breaking [2].

This indicates that with current theoretical knowledge only non-photochemical effects can describe the observed nucleation behavior, enabling Garetz et al. to name the phenomena Non-Photochemical Laser Induced Nucleation (NPLIN) [1]. Over the course of the past two decades, more evidence was found to believe that NPLIN is a true non-photochemical effect. A polarization switching window, in which the polymorphism was dependent on the polarization of the laser was observed. This behavior can be described by the Optical Kerr Effect which provides further evidence that the mechanism is non-photochemical [22].

Another important notion is that neither the solute nor the solvent has any or very low absorption bands at the laser wavelengths [29]. This means that the compounds will not absorb any laser photons and are thus transparent to the incident light. The lack of absorption reduces the likelihood of energy to be transported from the laser into the molecule.

The NPLIN effect shows a strong intensity dependence and a weak wavelength dependence [29], which is another indication that the laser induced nucleation is probably non-photochemical. Different wavelengths were tested on the same molecules and the results show nearly similar outcomes [25]. This means that the molecules still nucleate if enough energy is provided, despite the absence of the absorption bands.

The last evidence supporting the non-photochemical performance is the polarization switching window found by Garetz et al. [21]. The research group was able to obtain different polymorphic forms by adjusting the polarization from linear to circular. Figure 1.2 shows the laser polarization switching as performed by a quarter waveplate. As can be seen, the orientation of the laser light changes from linear to circular. It is assumed that the polarized light tends to align the molecules in such a way that it favors the formation of a particular polymorph [21].

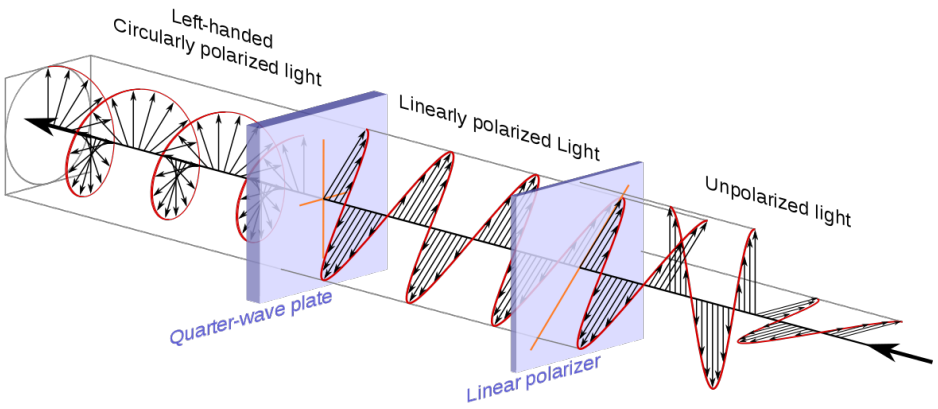

Figure 1.2: Circular and linear polarization visualized [30]

Various research groups have come up with fundamental explanations for this phenomenon called NPLIN. Interpretation of the first results raised the Optical Kerr Effect (OKE) as a reasonable explanation for the observed characteristics by Garetz et al. [1]. KCl has no particular bonds to be aligned in the manner envisaged by the optical Kerr effect, an alternative explanation based on the isotropic polarizability of pre-nucleating clusters, was proposed [13]. The initial model was expanded with the enhancement of nucleation through the isotropic polarization of sub-critical nuclei by the laser irradiation. Up to date, these are the only two proposed mechanisms relating molecular properties of the crystalline compound to the laser irradiation.

Two other alternative reasons to describe the observed characteristics are the availability of nano-impurities and the creation of a shockwave inside the sample. In the case of nano-impurities, it is imposed that these particles absorb a part of the laser light increasing the temperature forming small vapor bubbles that serve as a seed for the nucleation [14, 17]. Another possible effect of the impurity made bubble is a concentration increase close to the surface of the expanding bubble that causes the nucleation. Shockwaves, known to be capable of inducing nucleation, create rapid disturbances and density fluctuations that cause the sub-critical nuclei to favor further growth. The shockwaves are produced by the high intensity of the laser [31].

1.3.1. Molecular properties

Explaining NPLIN with molecular properties reduces the fundamentals to one mechanism; Optical Kerr Effect and its expansion explained by Isotropic electronic polarization.

Optical Kerr Effect

Garetz et al. [1] was the first research group to observe Non-Photochemical Laser Induced Nucleation while performing second harmonic generation in solutions of urea and water. They noticed accidentally that crystals were formed when the supersaturated sample was exposed to high laser intensities. Furthermore, the orientation of the crystals was dependent on the plane of polarization of the incident radiation, suggesting an electric-field-induced effect. Employing vertical and horizontal polarization verified this observation. Which points to the existence of an optical Kerr effect where the incident electric field induces a dipole moment in the molecule as shown in figure 1.3. Simultaneously, a torque is exerted to the molecule which aligns the most polarizable axis parallel to the electric field [1].

As the observations of NPLIN were in line with the characteristics of this phenomenon, it was widely believed that an optical Kerr effect was capable of laser induced nucleation. However, the first attempts to build a model explaining OKE showed that the dipole moment of glycine, a molecule that was known to be sensitive to NPLIN, was far too small to create a rotational motion of glycine molecules when exposed to an optical frequency of $\sim 3 \times 10^{14}$ Hz [7]. It was even calculated that glycine molecules exposed to these powers are only capable of rotating with 1° and thus this power is far too small to account for the observed effects.

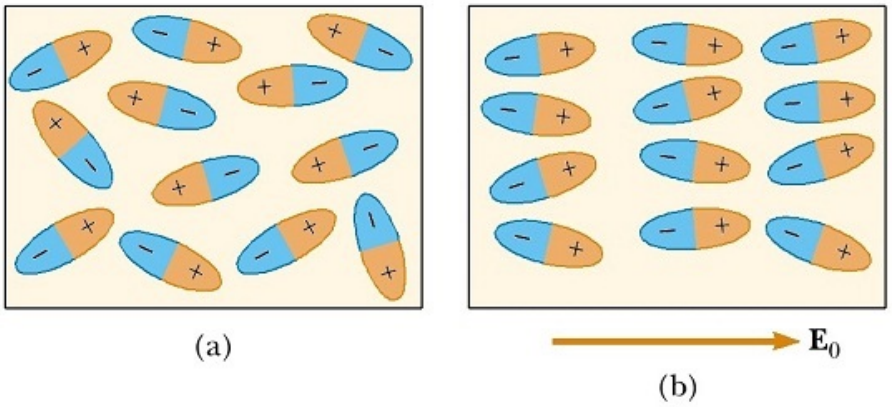

Figure 1.3: Polarization torque due to applied electric field [32], (a) initial stage where molecules are randomly distributed and not aligned, (b) visual of an applied electric field causing the molecules to orient and align accordingly.

Further research on OKE focused on collective effects amongst many molecules in a large cluster as a possible cause for the discrepancy between observed effects and the calculated powers [22]. By this approach, it is still reasonable to observe a minimum threshold energy for which the laser provides enough power to induce nucleation, which was the case. The differences in intensity thresholds for circular and linear polarization support the theory of OKE since it is more effective to align rod-like molecules of urea with linear polarization than with circular polarization. A follow-up by Duffus et al. [33] showed that supersaturated KCl solutions had not such a preference to circular or linear polarization. Dissolved KCl has no bonds to be aligned in the manner envisaged in the Kerr-effect and therefore an alternative mechanism was proposed, based on the isotropic polarizability of the pre-nucleating clusters.

Isoptropic electronic polarization
Isotropic electronic polarization (IEP), proposed by Garetz et al. [21], resulted in a further investigation by Alexander et al. [13] who provided a model and tested it experimentally. The main difference between IEP and OKE are the cluster effects; for OKE only one molecule is considered to be affected by the incident electric field as for IEP a sub-critical cluster of molecules is considered.

The new-built model showed that the Isotropic electronic polarization mechanism is useful to fit the obtained experimental data [13]. Sub-critical clusters are affected by the laser light which modifies the free-energy surface on which a small proportion of the clusters become supercritical, as shown in figure 1.4. However, the model still showed a large difference between the actually needed energy required to align the molecules such that they become supercritical nuclei and the observed experimental values to crystallize a KCl molecule within ns pulse widths [13].

1.3.2. External variables
Explaining the fundamentals of NPLIN providing OKE or IEP is not possible because of the discrepancies in theoretical and experimental approaches. Alternative explanations were based on external variables that did not include the molecule of interest, namely nano-impurities and shockwaves.

Nano-impurities
Due to the handling techniques when preparing samples for NPLIN experiments one cannot assure pure samples as small impurities are available in all used materials. The impurities can play a major role in the observation of NPLIN as these can lower the solubility and thus the supersaturation [34, 35]. Impurities can also have different absorption spectra compared to the solvent and solute, enabling high energy absorption rates. At last, these nano-impurities provide large surface-volume ratios opening the discussion for heterogeneous nucleation with increased crystallization kinetics [36].

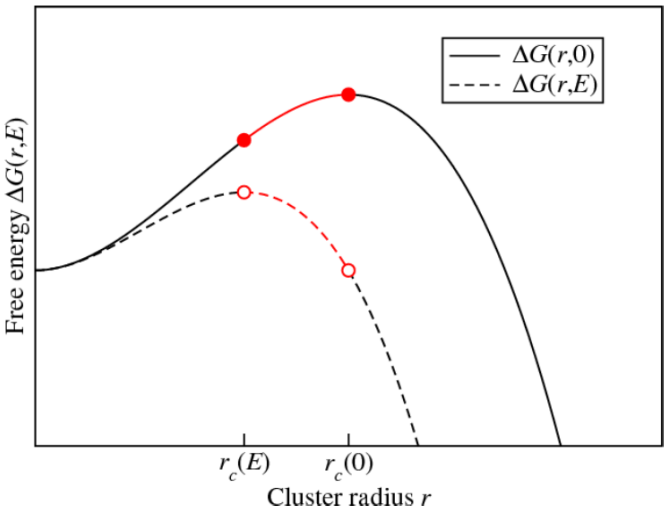

Figure 1.4: Schematic free energy curves. Clusters with critical radius $r_c(0)$ are affected by the energy provided by the laser causing them to lower to critical radius $r_c(E)$ making the range of clusters that exist within $r_c(0) \geq r \geq r_c(E)$ to nucleate [13].

Several researchers have looked into the effects of impurity-removal and impurity-doping. It was found that removing the impurities by filtration reduced the probability of laser induced nucleation significantly, however, does not stop the effect [13, 17]. Doping of these filtrated samples did recover the nucleation probability effects and enabled even better performance when extra molecules, such as surfactants, were added [14].

Extended theories were established upon the found correlations mentioning possible cavitation bubbles [29]. These cavitation bubbles have maximum radii in the range of $O(10^1)$- $O(10^3)$ μm and μs lifetimes, that collapse because of the unstable pressure. Previous research also showed that cavitation bubbles were inducing solidification of supercooled liquid water being an intermediate in the process. Nano-particles can be either an inhibitor or an unimportant factor in this phenomenon. Impurities acting as an inhibitor, absorb the incident light heating up the environment and providing huge amounts of energy to the surrounding molecules, mainly water, that vaporize and create a short-lived bubble. This bubble provides either the surface for heterogeneous nucleation or causes large density fluctuations near its perimeter raising the local supersaturation such that spontaneous nucleation is inevitable.

Shockwaves
A final reasoning is developed to describe NPLIN-behavior as a follow up on cavitation bubbles. Shockwaves are created by the collapse of bubbles and cause large pressure waves that alter the local density. Various experimental studies involving shockwave induced nucleation have proved to work for supersaturated solutions [12, 31]. Another supporting finding is the laser intensity threshold, which is expected with such a shockwave. The higher the intensity, the higher the pressure wave.

Thorough research by Kacker et al. [25] has shown that a laser pulse is insufficient to cause significant pressure waves even at intensities higher than those mentioned in the literature. At intensities up to 77 MW/cm^2 the pressure waves did not reach more than 17 mbar. The same samples were exposed to higher pressure waves, ~200 mbar, without exposing them to the incident laser light and these were unaffected, making it unlikely to address NPLIN to shockwaves.

1.4. Radicals

As the name suggests, NPLIN is expected to be a non-photochemical effect. If the effect was to be photochemical, a physical bond of the molecule is broken by the high-intensity laser beam. Such a phenomenon would cause the formation of short-living glycine radicals that cause disequilibrium in the sample and induce nucleation. The near IR-wavelength at which no such a bond is affected is a reason to opt for non-photochemical effects. Another countering observation is the ability of the samples to

regenerate. Each sample that was redissolved after laser-exposure and exposed again showed similar performance. Which have been affected if photochemical reactions occurred since that would change the sample composition [1].

Radicals, as intermediates for a reaction, are for a largely unknown, as they have a life span of roughly $O(10^1)$- $O(10^2)$ ns [37]. Increasing accuracy and availability of laboratory equipment over the past decades opened the way to obtain more data and information about radical formations. For glycine decarboxylation, an extensive paper was published by Bonifacic et al.[37] giving a preliminary list of possible radical formations of glycine. Adding another list mentioned by Berger et al. [38] for the oxidation of glycine and it becomes clear that Reactive Oxygen Species (ROS) are very likely products of glycine deformation.

1.5. Thesis objectives

In the current situation, four different mechanisms are proposed as an explanation for the observed Non-Photochemical Laser Induced Nucleation. So far, none of these mechanisms is fully excluded as the evidence for none of them is not completely comprehensive. However, as for the shockwave induced nucleation, a good amount of evidence supports a negatively biased view.

Because shockwaves are not likely to be induced by the laser, this research will focus more on the remaining points. Furthermore, several ideas regarding previous research were raised obtaining the following subjects of concern, reformed in preliminary hypotheses:

- The observed Laser Induced Nucleation is Non-Photochemical;
- NPLIN behavior is unaffected by external factors such as glass shape, pH dependency, and sample deformation;
- Nano-impurities enhance the nucleation behavior of NPLIN.

Chapter 2 elaborates on presumed non-photochemical effects for NPLIN. External factors such as glassware in combination with polarization, pH, and sample decomposition are considered in chapter 3. Results on Nano-impurities effects on NPLIN are described in chapter 4. Concluding all results and observations, chapter 5 provides an extensive discussion and recommendations for further research.

2

Photochemical effects

Photochemical reactions are initiated by the absorption of energy in the form of light. Molecules absorbing light create transient excited states whose chemical and physical properties differ greatly from the original molecules. Photochemical effects are known to be useful for polymorphic control in crystallization according to Okutsu et al [39, 40]. However, for those experiments, it was known that the light photons had sufficient energy to cause ionization or create radicals that subsequently react to produce nuclei. This statement does not hold for current NPLIN research since laser-induced nucleation was discovered at wavelengths and powers not capable of inducing photochemistry [13]. Moreover, the NPLIN behavior was discovered using simple compounds such as NH_4Cl and KCl of which it is hard to envision what photoproducts are formed [14]. Multiple photoproducts can be derived from larger molecules, like glycine, of which ROS (Reactive Oxygen Species) is the most likely [37]. Further study into glycine and photochemical effects are required to connect the NPLIN name to the observed behavior. The hypothesis related to this part of the research is as follow: "the observed laser-induced nucleation in supersaturated glycine samples is non-photochemical."

2.1. Materials and methods

Radicals are known to be short-lived and their detection requires accurate and fast equipment. In this study, use was made of a fluorescent dye that attaches to several radicals of which hydroxyl is the prominent one. After reaction, the dye is excited at a certain wavelength and emits fluorescence at another. The intensity of the emitted light is correlated to the concentration of dye involved in the reaction.

First of all, the glycine solution was prepared without any purification. Glycine (Sigma-Aldrich, puriss, buffer substance, 99.7-101%, 33226) was dissolved in ultrapure water obtained via the purifier (Elga Purelab Ultra, 18.2 MΩ.cm) to prepare the supersaturated solutions. The supersaturations were determined based on the molality, which is expressed as mass of solute over mass of solvent. Molarity, describing the mass of solute over mass of solution is disregarded in this research. Glycine supersaturations of 1.5 and 1.7, corresponding to 367.5 and 416.5 gram per 1 liter water respectively, were used for radical measurements.

To maintain reproducibility, the following preparation steps were performed with the highest accuracy and carefulness. First, a stock solution was prepared by weighing the required amount of glycine in a borosilicate glass bottle. After weighing the glycine, a pre-calculated amount of ultrapure water was added using volumetric flasks. The cap was tightened as much as possible to ensure that evaporation could not occur when maintaining the stock solution in the oven (Binder Model FDL 115, 30-300 °C) at 65 °C for roughly 4 days to make the glycine dissolve.

As soon as the glycine was dissolved, the stock solution was transferred to circular vials (BGB, 8ml Screw vial (clear), 887040367423). The procedure was performed by placing a beaker on a regular hot plate (IKA RCT Basic hot plate) that remained at 65 °C equipped with a stirrer at 300 rpm. 300 ml stock solution was poured into the beaker and then transferred quickly to the vials using 30 ml syringes

(Fisher scientific, Plastipak 30 mL Luer syringe, 301231). After filling the vials up to the neck, all vials were closed by screwing the cap tightly. After 10 vials were filled they were put into the oven at 65 °C. This process was repeated until the entire batch was completed. The vials remained another week at this temperature before they were slowly cooled down to 24 °C over the course of 24 hours in a thermobath (Lauda Eco Gold, up to 200 °C). Another 2 days were used for waiting time, please consult appendix A for the terminology of the sample handling stages.

After the vial's temperature reached 24 °C, 2 to 8 μl of aminophenyl fluorescein dye (APF (Hydroxyl, hypochlorite or peroxynitrite sensor), ThemroFisher scientific, A36003) was added to each vial, resulting in a dye concentration between 1 to 4 μM. Subsequently, the vials were shaken gently to avoid crystallization but ensure full mixing. The vials were then dried using tissue and put on top of the sample platform in the set up as indicated in figure 2.1 at point 2.

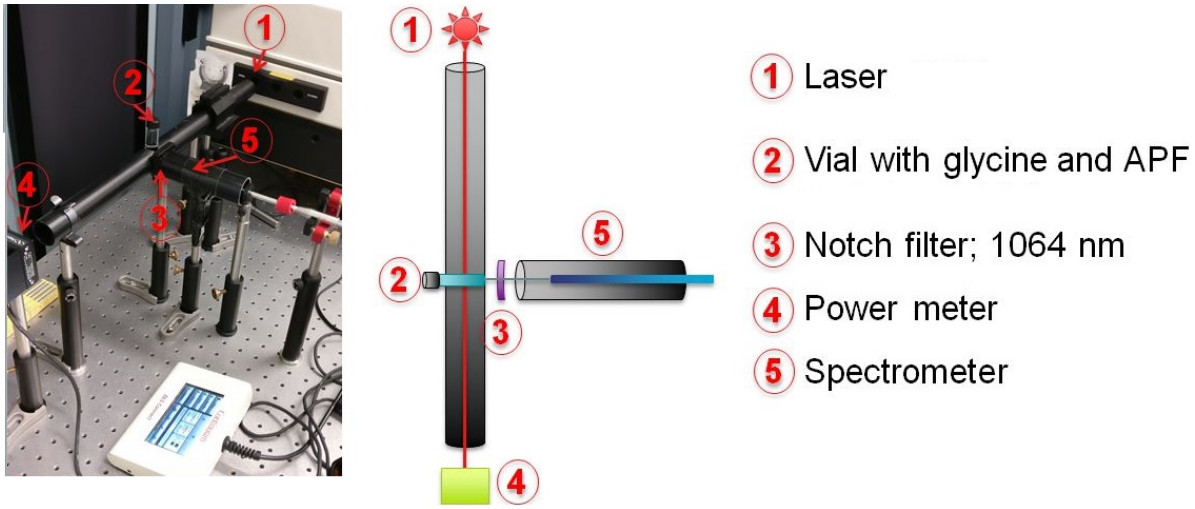

Figure 2.1: Laser set-up for radical measurements. The fundamental 1064 nm laser beam could be converted into 532 or 355 nm. A power meter was used to ensure the same power output over several experiments. The spectrometer was installed to measure emitted fluorescence.

Each vial was exposed one-by-one to the Q-switched Nd:YAG laser (Continuum Powerlite DLS 8000 model). This laser generates a train of 7 ns linear polarized light pulses at the repetition rate of 10 Hz and a fundamental wavelength of 1064 nm. The laser beam has a diameter of 9 mm and provides roughly 10 W of energy, resulting in a laser intensity of 220 MW/cm^2 at standard operation. When the laser beam passes through high harmonic generation crystals, the fundamental wavelength is converted to 532 or 355 nm, reducing the power output to 3.2 and 2.8 W respectively. A power meter (Newport 818P-030-19) was used to measure the output power of the laser beam. The spectrometer (Hellma detector, ocean optics HR2000+ CG-UV-NIR) was used to measure the light spectrum from 100 nm to 3000 nm in real time close to the exposed vial.

2.2. Results

Several experiments have been performed to measure if any photochemical effects were observable. Over the course of the experiments it was found that, due to supersaturated solutions and the introduction of an extra chemical, it was hard to find an experimental procedure capable of keeping the sample stable for use. This subsection describes the development of the experimental procedure, including all conclusions drawn throughout the process.

Self-made set-up as showcased in 2.1 was built before each experiment. In order to check the stability of the dye-glycine complex, use was made of 1064 nm laser pulses, as the corresponding power output is known to be an effective nucleation promoter for glycine at supersaturation 1.5. Spontaneous nucleation happened in 80% of the vials directly after the dye was added. The remaining 20% was kept at 24 °C for a few minutes to ensure stable samples. If the sample remained dissolved, it was

exposed to the laser for a minute (~600 pulses). Nucleation occurred within a few hours and no other phenomena like fluorescence were observed. This indicated that introducing the dye would not affect the nucleation behavior in terms of visual interpretation.

2.2.1. Hydrogen peroxide

As no fluorescence was detected, it was required to perform a reference measurement where the APF dye would react with the hydroxyl radical immediately. Since hydroxyl radical is presumed to be non-existent during NPLIN with glycine, hydrogen peroxide (H_2O_2, hydrogen peroxide 30% for analysis EMSURE, 107209, Merck) was used as a test chemical. H_2O_2 is known to produce the hydroxyl radical when exposed to UV (ultra-violet) radiation, having a peaking at ~210 nm [41]. The dye, on its turn, reacts immediately with the formed hydroxyl radical and emits fluorescence after being excited by wavelengths lying within the UV spectrum, peaking at ~490 nm. Of the available wavelengths; 355, 532 and 1064 nm, only 355 nm is fit for producing the hydroxyl radicals. Since 355 nm is far from the 210 nm peak for effective hydroxyl radical creation, it is expected that only low hydroxyl concentrations are generated. To create significant concentrations and to excite the dye right after, it was chosen to expose samples to a train of 600 pulses.

During exposure, the spectrometer appeared to be incapable of measuring any fluorescence emitted by the dye. The background noise of the ambient light and the low fluorescence signal by the dye hampered the reliability of the measurement. However, the fluorescence of the dye was strong enough to be observed by the naked eye. After performing a series of experiments with vials containing: water only, water with dye (concentration 1-10 μM), H_2O_2 only and H_2O_2 with dye (concentration 1-10 μM), the fluorescence was apparently caused by the excitation of hydroxyl-dye product. Provided with this information it is known that a small amount, yet undefined, of hydroxyl radical is enough to make a visible cloud of fluorescence inside the vial.

2.2.2. Glycine radical

The current setup enabled insights in the formation of hydroxyl radicals and thus glycine samples were ready to be checked. Performing a high nucleation rate at 355 nm requires either high power intensities or high supersaturations as was found in intermediate experiments. To make sure that the sample would nucleate after exposure, such high intensity or supersaturation was necessary. An ~65 MW/cm^2 is the maxim intensity that can be obtained at 355 nm and for that reason, it was chosen to use a supersaturation of 1.7 instead of 1.5. Such an increase in supersaturation also increased the spontaneous nucleation rate directly after adding the dye. To circumvent this issue all vials were warmed up to 37 °C, as this is the highest known temperature for APF to remain active. After reaching 37 °C the dye was added and all vials were cooled down to 24 °C again over a period of 2 hours. Following this method, 20% of all vials remained unaffected and were ready for exposure.

During exposure two different types of samples were used for comparison; supersaturated glycine solution S=1.7 and supersaturated glycine solution S=1.7 containing 2-10 μM dye. The experiments were performed by exposing the samples to laser pulses at 355 nm for a minute. The vials were exposed shortly after another to make the best possible comparison. There was no significant difference to be observed between all exposed vials. All vials nucleated within a few minutes, meaning that the laser beam was strong enough to induce NPLIN. This observation follows the initial thought raised by Garetz et al., describing the LIN behavior as a non photochemical effect.

3

External factors

Various factors affect the relation between laser irradiation and induced nucleation. In former studies, several methods have been applied to verify if NPLIN also occurs in completely different experimental set-ups, such as a levitated droplets [23] and square glassware [12]. These experiments were all completed with success, meaning that NPLIN is not dependent on these so-called external variables. However, it was found that some of the parameters affected the NPLIN characteristics in either a positive or negative manner. Such findings require more in-depth research to create the most optimal NPLIN performance when applied on larger scales. In this chapter, research into the effects of glass geometries, pH, and the color changing of glycine solutions is addressed.

3.1. pH dependency

Early research focused mainly on the dependency of NPLIN on intensity and supersaturation which were regarded as possible indicators for the Optical Kerr Effect [7, 21]. Later studies revealed that polymorphism can be controlled by means of laser adjustments [11]. Only one article mentions the pH as an important factor that plays a key role in glycine polymorphic existence [42]. pH affects the way how glycine crystals are being formed, as glycine is a zwitterion that changes molecule structure at different pH values [2]. It is known that (gamma-) γ-glycine formation is inhibited at pH below 4 and above 8, while (alpha-) α-glycine is dominant at a pH of 6 [43]. Therefore, glycine serving as a role model for the polymorphic control requires further research on pH-dependent NPLIN.

3.1.1. Materials and methods

Throughout the thesis project, several remainders of stock solution were checked for their pH value, using a pH meter (914 pH/Conductometer, Metrohm). The measurement was carried out by waiting until the pH value stabilized. Further investigation was required as the pH of the used purified water differed in a range from 5.5 to 8. 8 glycine stock solutions of ~25 mL were prepared with supersaturations 1, 1.1, 1.3, 1.4, 1.6, 1.7, 1.9 and 2 (at 24 °C) by adding 4.9, 5.39, 6.37, 6.86, 7.84, 8.33, 9.31 and 9.8 gram glycine (Sigma-Aldrich, puriss, buffer substance, 99.7-101%, 33226) respectively to 20 mL of ultrapure water obtained via the purifier (Elga Purelab Ultra, 18.2 MΩ.cm). Solutions were prepared in 50 mL centrifugal tubes with an orange cap (Corning 50 mL self-standing centrifugal tube, 430921) and left in the oven at 70 °C over the course of a week to reach complete dissolution.

After glycine was fully dissolved, the vials were taken out of the oven and pH measurements were performed immediately. Due to high supersaturations at 24 °C, it was necessary to measure the samples while they were still hot enough to prevent heterogeneous nucleation on the pH probe. Even at 70 °C, heterogeneous nucleation was inevitable for supersaturation 1.9 and 2, so pH values were not obtained. After completing the measurements at high temperature, the samples were placed back in the oven to ensure full dissolution before performing new measurements at 24 °C. After another day in the oven, the pH measurements were performed at 24 °C, by cooling the vials for 3 hours at room temperature.

3.1.2. Results

Aforementioned experiments were performed once and the results, as shown in 3.1, ruled pH effects out for the observed polymorphic behavior in NPLIN. The pH of glycine samples was measured to be around the value of 6 ±1, which is still highly favoring α-glycine in spontaneous nucleation [43]. Even when pH-values of ultrapure water varied, the pH of the glycine stock solution remained around 6. Such behavior can be explained by the buffering capabilities of glycine. When dissolved in water, glycine acts as a buffering agent that keeps the pH somewhat constant, ±1. When other compounds are introduced, this behavior can be elevated to another pH value, where it starts buffering around its new equilibrium pH. The effect of the pH of ultrapure water was found to be ineffective to create such elevation. In the first part of the research, the pH was measured for every stock solution. After preparing more than 10 different stock solutions, this stage was skipped, as pH was concluded to be constant.

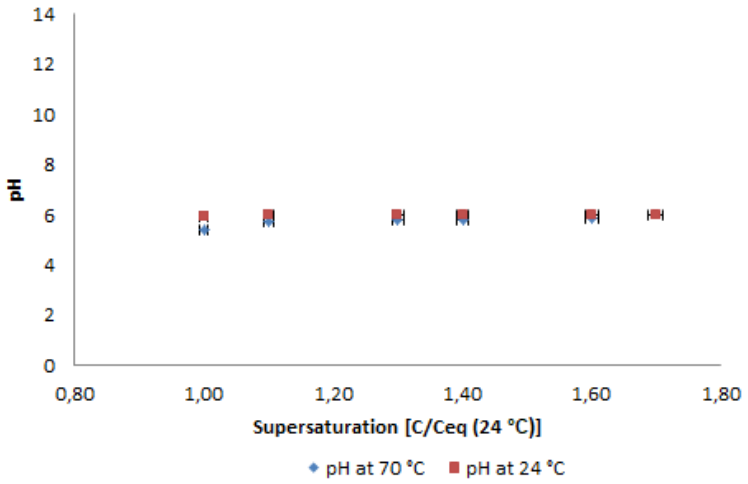

Figure 3.1: pH values for different glycine stock solutions at different supersaturations. pH is measured at different temperatures to avoid spontaneous nucleation. Error bars represent the error of weighing water and glycine, resulting in a different supersaturation.

3.2. Sample coloration

Through the course of this research, it was observed that samples, that initially were clear, started to become yellow the longer they were used. An example of this phenomenon is showcased in figure 3.2. Glycine was dissolved in pure water and no other compounds were added afterward. No other article describes the color-changing behavior of glycine, neither in NPLIN related articles or glycine related research. In order to know whether the color change has an effect on the NPLIN behavior, further research into the cause of it is done.

Figure 3.2: Three vials containing dissolved glycine at a supersaturation of 1.7. The most left vial has been in the oven for a few months, the centered vial has been used for a few weeks and the most right vial is new and fully transparent.

3.2.1. Materials and methods

Multiple glycine samples have been tested during the study. The samples were prepared as described in the materials and methods sections with supersaturations ranging from 1.5 to 1.7. All samples used were fully dissolved and cooled down to room temperature before the examination.

Different types of equipment were used to examine the colored samples. The UV-Vis spectrum of the ”old” glycine was measured and compared to that of the transparent samples, that were recently prepared. Additional experiments employing Fourier-transform infrared spectroscopy (FTIR) spectroscopy were carried out to determine the molecular structures of the sample. At last, an ion-chromatograph detected specific ion concentrations.

For the examination of the sample, an Ultraviolet-visible (UV-vis) spectroscopy device (Hach, DR6000^{TM}) was used. Samples were transferred from the vial to the cuvette (UV range cuvettes 4 clear sides, Kartell labware, 01961-00) using a disposable pipette. The first cuvette is used as a reference sample as the absorbance of this sample is subtracted from the other measured absorbances during that run. For this reason, a reference sample was chosen to contain water, as all other samples were water-based. Thorough usage learned that empty cuvettes showed a different absorbance graph, as there were 4 distinct interfaces through which the light was passed. In the case of water-filled cuvettes, the number of interfaces was reduced to 2 as the interface between glass and water is negligible in terms of absorbance.

The infrared spectrum was recorded using an FTIR device (Mettler Toledo, ReactIR 15) which measured the IR spectrum every 15 seconds. FTIR examination was performed inside the vials as they were wide enough to fit the FTIR probe in.

The last device used, the ion chromatograph (Dionex, DX-120 Ion chromatograph), consisted of an anion column that was used to measure the quantities of positively charged ions inside the sample. The samples were diluted 10 times with ultrapure water before being inserted into the chromatograph.

3.2.2. Results

After performing the pH measurements, part of the samples was kept in the oven for use at latter stage. These samples turned yellow over the course of a few months and ruled out two factors possibly responsible for the coloration. The pH samples were held in centrifugal tubes instead of the regular borosilicate vials, meaning that neither impurities from the vials nor the PTFE cap were causing the yellow color. Another important note was the fact that these samples were not exposed to the laser light, thus excluding the possibility of laser-induced color-changing effects.

For the UV-Vis spectroscopy, different measurements were performed. Both supersaturation 1.5 and 1.7 were checked using samples that were relatively new (one week) and still transparent, as well as samples that were a few weeks or months old that turned visibly yellow. For supersaturation 1.7 this yellow color had a huge effect on the spectroscopy as shown in figure 3.3. This figure clearly indicates that a new sample shows only half of the absorbance below 500 nm compared to a sample that is a few weeks old (3-4 weeks) and even 1/7 of the absorbance of a months old (3-4 months) sample. Repeating the same measurement for multiple samples at these three stages defined a clear increase of absorbance over time. It is likely to assume that the solution degrades over time and a new compound is formed which is responsible for the change in color. However, no particular compound was found to be related to this increase of absorbance in the 250-450 nm range. To investigate what chemical could cause sample coloration, FTIR equipment with built-in database was used.

FTIR spectra consisted of many peaks in the 2500-15000 nm range. The integrated software enabled the selection of each peak and the connected database proposed the bond identification based on the position of the peaks in the spectrum. When comparing the FTIR spectra of both yellow and transparent samples, there were no distinct peaks or valleys observed. After repeating the measurement several times, it was concluded that the compound causing the yellow color is not absorbing at IR wavelengths. Therefore the FTIR was not capable of determining the possible chemical that caused the color shift.

The last examination, ion chromatography, was used to look at particular ions. During the research, several causes were proposed of which ammonium (NH_4^+) and iron were the most promising ones. Ammonium is known to be one of the impurities of the glycine used and it is also one of the bonds available in glycine. Heat could increase the dissociation speed for an amino acid as the pH slowly changes [44], creating larger amounts of NH_3 that become NH_4^+ in acidic environments (pH <7). The iron idea was generated by doping the sample with iron nanoparticles, as will be described in section 4.1, where samples turned slightly yellow after adding the iron nanoparticles. Together with data from former research [45] a formation of compounds such as $FeOH^{2+}$ seems likely.

The ion chromatograph results corresponding to samples used in figure 3.3, are shown in table 3.1. After several measurements, it became clear that iron is present in the samples but in very limited

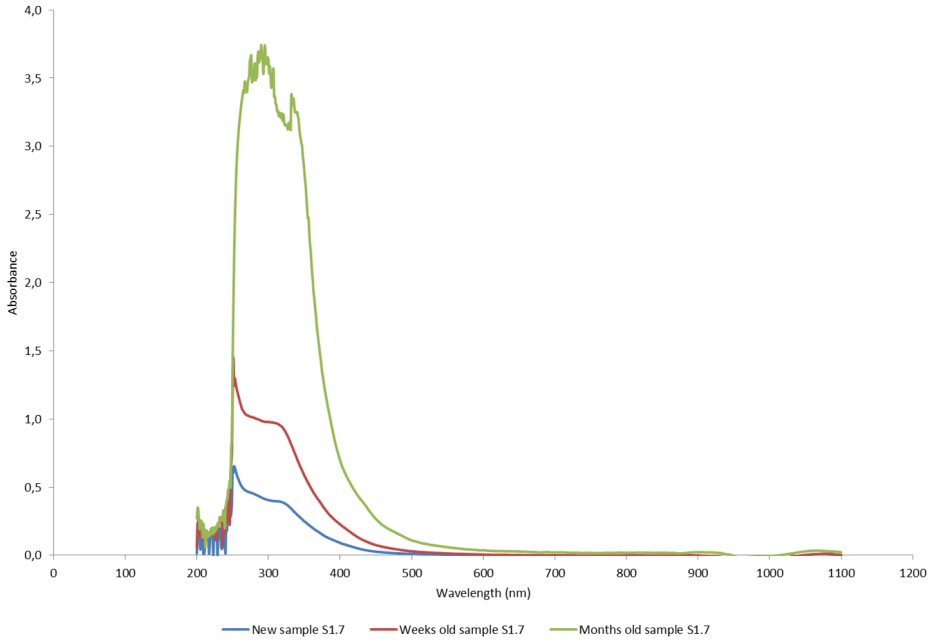

Figure 3.3: UV-Vis spectrum of 3 glycine solutions at supersaturation 1.7 that were prepared at different times during the research. The large fluctuations below 250 nm are caused by the cuvettes, as these become more absorbent at these wavelengths. The valley around 908 nm is accounted to a high concentration of glycine, reducing the water concentration, while the reference sample was fully water.

amounts which can not account for the coloration of glycine solution. Ammonium, however, shows a clear increase in concentration with time. Because all the vials tested showed an increase in ammonium together with a more visible yellow color, it can be concluded that with current insights this color is proportional to the availability of NH_4^+. The reduction of glycine concentration, due to the formation of NH_4^+, is calculated to be negligible in case of the ~8 ml samples that were used. Moreover, the decrease in supersaturation after a period of a few months was calculated to be only 0.009.

Table 3.1: Ion chromatography results for glycine samples

Sample	iron [ppb]	(NH_4^+)
New sample S1.7	70	34
Weeks old sample S1.7	70	61
Months old sample S1.7	70	593

3.3. Glassware

As mentioned in the introduction of this chapter the glassware shape appears to affect the nucleation behavior. Earlier research revealed that laser-induced nucleation probability depends mostly on the laser intensity [29, 46]. Cylindrical vials act as a focusing lens increasing the beam intensity by twofold inside the sample [22], therefore serving as an explanation for lower nucleation probabilities for square container geometries at constant power output.

Besides the intensity difference, one could argue the observed polarization switching windows. Previous studies mentioned a polarization switching window where light of different polarizations (linear and circular) was able to produce different polymorphs [11, 12]. All these discoveries resulted from experiments using cylindrical borosilicate glass vials. Circular geometries can cause the outside section of the laser beam to be reflected as it gets closer to the Brewster's angle. As the light comes closer to the Brewster's angle, the more the light becomes polarized, meaning that the initial polarization is partly adjusted into a more elliptical shape [30]. Such an effect would cause large polarization differ-

ences inside the sample for the different tested vials and make them incomparable. For this reason flat geometries, as in square containers, are to be tried to observe the same polarization window as initially observed by Sun et al.[11]. To define the purpose of this subsection the following hypothesis is raised: "Glycine polymorphism is dependent on the polarization switching for both flat and circular geometries." Additionally, it is reviewed whether this effect is stronger for flat geometries since the polarization is adjusted the least by the flat surface of the vial.

3.3.1. Materials and methods

Glycine (Sigma-Aldrich, puriss, buffer substance, 99.7-101%, 33226) was used without any purification. Glycine was dissolved in ultrapure water obtained via the purifier (Elga Purelab Ultra, 18.2 MΩ.cm) to prepare a supersaturated solution. One supersaturation was used to perform the experiments, 367.5 gram glycine per 1 liter of ultrapure water, resulting in a supersaturation of 1.5 at 24 °C (Solubility at 24°C is 245 g/L). For the glassware experiments, three vials were tested: circular 8 ml (BGB, 8ml Screw vial (clear), 887040367423), circular 16 ml (BGB, 16ml Screw Vial (clear), 887040379796) and square 15 ml (Fisher scientific, fisherbrand clear french square bottles with black phenolic polycone cap, 11768749).

To maintain reproducibility, the following preparation steps were performed with the highest accuracy and carefulness. First, a stock solution was prepared by weighing the required amount of glycine in a borosilicate glass bottle. After weighing the glycine, a pre-calculated amount of ultrapure water was added using volumetric flasks. The cap was tightened as much as possible to ensure that evaporation could not occur when maintaining the stock solution in the oven (Binder Model FDL 115, 30-300 °C) at 65 °C for roughly 4 days to make the glycine dissolve.

As soon as the glycine was dissolved, the stock solution was transferred into the square and circular vials. This was performed by placing a beaker on a regular hot plate (IKA RCT Basic hot plate) that remained at 65 °C equipped with a stirrer at 300 rpm. 300 ml of stock solution was transferred quickly to the vials using 30 ml syringes (Fisher scientific, Plastipak 30 mL Luer syringe, 301231). Vials were filled up to the neck and closed by screwing the cap tightly. After 10 vials were filled they were put into the oven at 65 °C. This process was repeated until the whole batch was filled. The vials remained another week in the oven before they were slowly cooled down to 24 °C over a course of 24 hours in a thermobath (Lauda Eco Gold, up to 200 °C). Another 2 days were used for waiting time, please consult appendix A for the terminology of the sample handling stages.

After 2 days at 24 °C the vials that nucleated spontaneously were removed from the batch and were not incorporated with the nucleation probability. The spontaneous nucleation appeared to affect only 1-5% of the batch that contained between 80 and 100 vials. The remaining clear vials were dried using tissue and exposed one-by-one to the Q-switched Nd:YAG laser (Continuum Powerlite DLS 8000 model). The laser generates a train of 7 ns linear polarized light pulses at the repetition rate of 10 Hz and a fundamental wavelength of 1064 nm. The beam diameter is 9 mm and has a power output of 10 W, resulting in a laser intensity of 220 MW/cm^2 at standard operation. Each sample was exposed to the laser light slightly above the bottom of the vial (∼4 cm) through the glass-liquid interface. After exposure, each vial was placed quickly back into the thermobath to remain a constant temperature of 24 °C inside the vial. Another 24 hours was used before all vials were inspected for nucleation probability and polymorphism because this point was found to provide the most stable nucleation probabilities in the shortest amount of time [27].

In the first few experiments polymorphism was identified by using an X-ray diffraction (XRD) device (Bruker D2 Phaser). Each vial containing crystal particles was emptied by pouring the remaining liquid into the corresponding waste container. Because of the crystal adherence to the glass surface, it was necessary to wrap the vial in tissue and to crush the glass in order to retain the crystal. Each crystal was then dried by applying nitrogen and crushed using pestle and mortar. After grinding each sample they were introduced to the XRD that provided a plot which was compared with the fundamental plots of the glycine alpha, beta and gamma polymorph [47–50]. By comparison, it was determined what polymorphs were obtained. After performing over 300 XRD runs, it became apparent what visual characteristics applied to each polymorph.

3.3.2. Results

The results consist of several experiments performed with the two types of circular containers of 8 and 16 ml and the square container of 15 ml. The unavailability of smaller square vials required the use of larger circular vials, namely the ones of 15. This inconvenience led to two extra variables that were checked. Both the exposed volume increased and the laser-interaction surface was flatter as the diameter of the big vials increased. By doing so more insight was gathered about the effects between larger and smaller containers as well as the shape of the geometry. Such information can be very useful when scaling the NPLIN process as using the right laser-solution interface could enhance the NPLIN behavior and might increase plant operation yields.

While performing the experiments, two output parameters were measured, polymorphism and nucleation probability. The results of these parameters by adjusting the available variables, polarization and container geometry, are shown in figure 3.4. The other experimental parameters, such as room temperature, laser power and distance between laser and sample remained within 5% for each experiment.

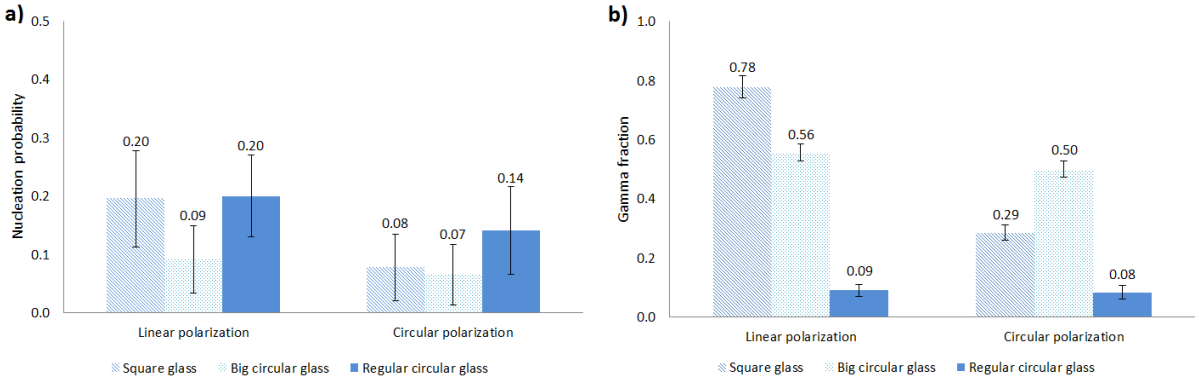

Figure 3.4: Results of glass geometry experiments using irradiation of a single pulse at 1064 nm and an intensity of 220 MW/cm^2 for glycine solutions at supersaturation 1.5. Figure a) presents the nucleation probability for the adjusted control parameters. 95% confidence intervals show the certainty of the experiments [51]. Figure b) visualizes the polymorphic change by adjusting polarization and glass geometries for laser exposure.

Figure 3.4 a) indicates equal nucleation probabilities for all vial geometries regardless of the polarization because all error bars partially overlap. Similar results were reported also by Alexander et al. [13] and clearly indicates that nucleation probability is not dependent on the polarization switching or the shape of glass-laser interface. Slight differences between circular and square glass were expected as the beam intensity inside the circular vials would be higher, due to a converging path caused by the lens-like behavior of the vial. Previous research showed that nucleation probability was mainly dependent on the laser intensity and solution supersaturation [13].

Figure 3.4 b) shows a significant difference between glass geometry and polarization effects for polymorphic output. As mentioned in previous research [27] no remarkable difference in polymorphic structure is observed in circular containers when the polarization is switched. Aforementioned research aimed at switching effects in 8 ml circular vials. In this study, it is confirmed that the polymorph does not change due to polarization switching when using circular vials. However, a polymorphic difference between small and large circular vials is found. γ-polymorph is favored in larger volumes with a larger curvature radius. Such behavior can indicate that γ-glycine, which is known to be less structured, is more likely to occur when a larger volume is exposed to laser irradiation. As a result, multiple crystal seeds were created and a less organized structure results in the formation of glycine.

Another observation for figure 3.4 b) is a clear difference in γ-glycine probability when square containers were used. As explained in the introduction of this chapter it is expected that circular vials affect the circular polarization of the laser beam into more elliptical shapes. Such an effect is not expected for flat surfaces. The results presented in 3.4 b) support the reasoning by Sun et al. [11], where a fully circular and linear polarization indeed cause different polymorphic crystal structures.

The initial hypothesis ”Glycine polymorphism is dependent on the polarization switching for both flat and circular geometries” is by means of the aforementioned results partly rejected. The hypothesis holds for flat geometries, as polarization switching is causing polymorphic changes. However, for circular geometries, it was found that adjusting the polarization did not affect polymorphic outcomes, likely to be caused by the glass-laser interface effects.

4

Laser irradiation effects

After establishing a sound fundamental idea about several non-investigated factors, as discussed in chapter 3, in-depth research is required into topics that were already related to NPLIN. Current in-house research focuses on the existence of a cavitation bubble which is closely related to the phenomena described in section 1.3.2. These cavitation bubbles are expected to emerge following the energy absorption by either the solvent or the impurities present in the sample. Because the solution is transparent at used wavelengths, it is more likely to opt for impurity-based bubbles. This chapter will elaborate on the effect of the impurities, as they are known to be a major promoter of NPLIN [14], and describes the effect of laser-sample volumes, raised in section 3.3.

4.1. Impurities

Impurities are known to stimulate nucleation in general. They reduce the stability of solutions, making them more susceptible to nucleate [34, 35]. Also, heterogeneous nucleation is more likely to happen at a larger concentration of impurities as additional surface which acts as a promoter, is added. In the case of NPLIN, it is expected that impurities have an even more important role because they can absorb some of the laser light providing the energy to overcome the sub-critical nucleus size. This section serves the hypothesis: "The type and the concentration of nano-impurities promote laser induced nucleation behavior."

4.1.1. Materials and methods

Different setups were used over the course of this section. The experiments consisted of two experimental layouts, designed for both linear and circular polarization. Besides, a variety of parameters was tested: impurity concentration, wavelength, type of impurity and supersaturation. To check each parameter individually, all other parameters were maintained at the constant value.

Glycine solutions were prepared as described in chapter 2. However, when sample doping was required impurities were added to a fully dissolved stock solution and transferred into vials. The impurities, silica nano-impurities (20 nm Silica nanospheres, nanoXact^{TM}, nanocomposix, JRC0080) or iron oxide nano-impurities (Iron (II,III) oxide 25 nm nanoparticles, 900201-2 ML, Sigma Aldrich) were added by pipette, at the required concentration related to the total solution volume. Before adding the impurities, it was necessary to put them in an ultrasound bath (2510 Branson) for 5 minutes.

When filtration was required, syringe filters (0.45 μm) were used to retain the micro-impurities inside the syringe (Terumo 10 ml Syringe Luer lock) while transferring the liquid into the vials. To ensure that no glycine was trapped inside the syringe filters some vials were dried and weighed. The results concluded that the amount of glycine was the same in each vial, either filtered or not.

The experimental setup for linear polarization only requires a laser beam and an elevated platform on which the vial rests. The laser produces 10 W of 1064 nm linearly polarized light at standard operation. A second harmonic crystal is used to convert the wavelength from 1064 nm to 532 nm, while

polarization is flipped by 90° but still linear. A quarter waveplate ($\lambda/4$ @1064 nm, Thorlabs) was used to transform the polarization from linear to circular, as indicated on point 2 in figure 4.1. A Glan-Taylor polarizer (GL10-A, Thorlabs) was employed to inspect the quality of the circularly polarized beam as shown in figure 1.2.

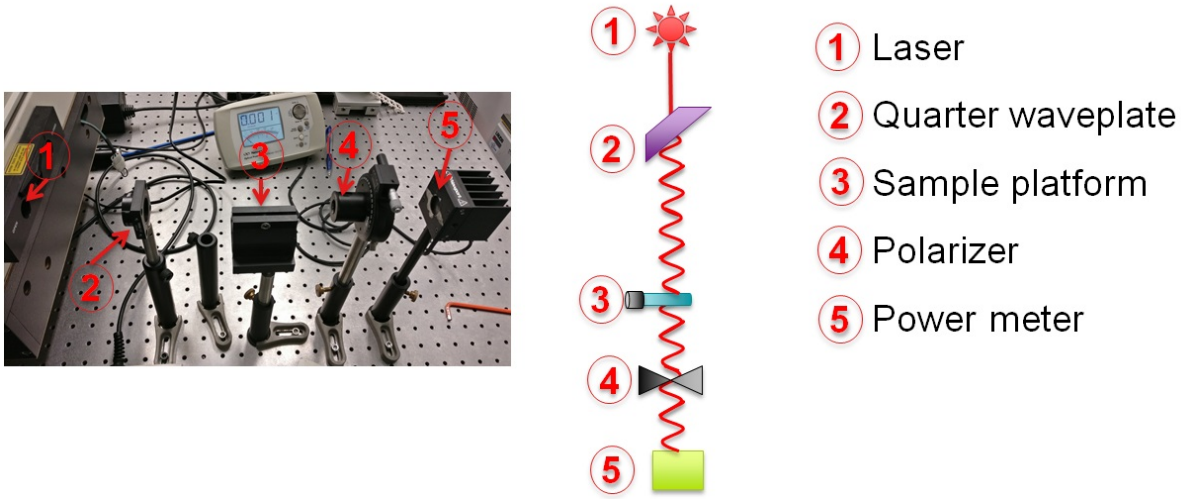

Figure 4.1: Experimental build for impurity experiments. Part 4, the polarizer, is used for accurate circular polarization and is checked by the power meter, point 5. During the actual exposure, this polarizer is removed as it no longer serves a purpose.

To derive conclusions on the nature of the doped glycine samples use was made of a Zetasizer (Malvern zetasizer nano zs) capable of measuring particle size distributions (PSD) in liquid samples. Specific cuvettes (Disposable Cuvettes PMMA semi-micro, 634-0678, VWR) were filled with 350 ml of sample, either pure or diluted 2-5 times with water. The cuvettes were placed inside the Zetasizer at room temperature. For each sample, the device automatically calculated the required amount of runs to measure a stable sample. After running this automatic sequence, each sample was measured another time to ensure similar outcomes. Using the equipment software, information about the intensity, volume, and number distribution were obtained. Further detail can be found in appendix C.

Since impurities can affect absorbance in NPLIN experiments, UV-vis equipment was used. The procedure can be found in section 3.2.

4.1.2. Results

Five distinguishable samples serve as the foundation for the impurity experiments, all based on glycine supersaturation 1.5. The first sample is just glycine aqueous solution without further purification or contamination steps. The other 4 samples are supersaturated glycine (S=1.5) samples as well but doped with either silica or iron oxide impurities. Silica impurities were chosen because they are not electrically charged and are likely to act neutrally inside the sample, serving only as an impurity. The concentration of silica was chosen to be between 5 and 100 ppm. 5 ppm was selected initially to mimic the impurities already present in the glycine solution. A 20-fold increase in the second batch was used to find if there was a significant difference in nucleation probability at the new concentration. The elevation in impurity concentration does not increase absorbance at the used wavelengths (532 and 1064 nm) as can be seen in appendix D. The particle size distribution depicted in appendix C, clearly shows a peak at ~25 nm which is ascribed to the nano-impurities.

Iron oxide, on the other hand, is known to cluster with certain components inside the solution as it becomes charged due to pH fluctuations [14]. Because iron is a common impurity in several chemical compounds that have been used to prove NPLIN, it is chosen to use a concentration in the same range, namely 5 ppm and 20 ppm. Just as with silica, the iron oxide concentration does not contribute significantly to the absorption rates measured at the two used wavelengths (532 and 1064 nm), as shown in appendix D. Similar to the report of Ward et al. [14], iron oxide nanoparticles are found to

cluster to sizes of the order of hundreds of nanometers, see appendix C.

All aforementioned samples were tested at both linear and circular polarization and the results of the nucleation probability are shown in figure 4.2. It can be clearly derived that linear polarization has an increased nucleation probability compared to circular polarization for some of the doped samples at 1064 nm. Previous NPLIN studies revealed that the supersaturation dependent nucleation probability was more effective for linear polarization than for circular polarization. Adding impurities generates similar behavior as increasing the supersaturation. This phenomenon would suggest that more impurities decrease the solubility of glycine and therefore enhance the supersaturation to a more critical level where the laser provides the energy for nucleation.

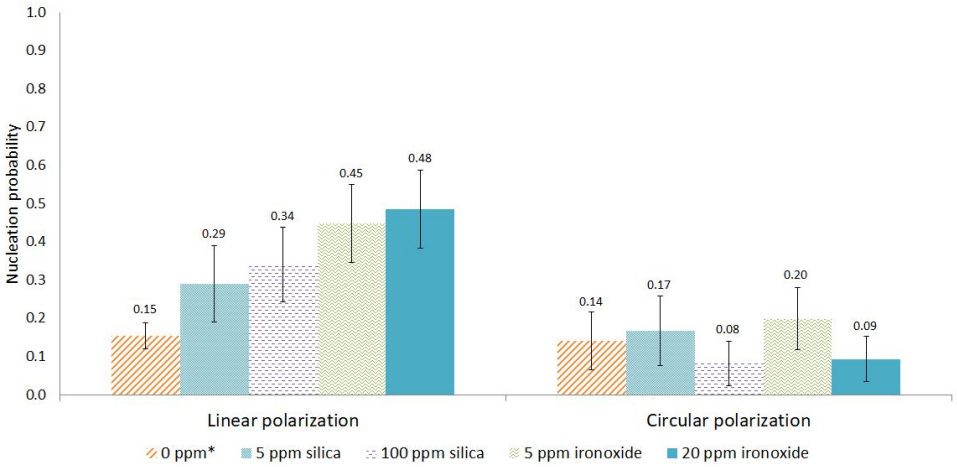

Figure 4.2: Results of impurity doped samples for 1 pulse irradiation at 1064 nm and an intensity of 220 MW/cm^2 for solutions at supersaturation 1.5. Vials were counted 24 hours after exposure. 95% confidence intervals show the certainty of the experiments [51]. *0 ppm glycine solutions were not doped with impurities

To create a full overview of the effects of impurities, the filtration process was also performed. Because supersaturation 1.5 is already on the low end of nucleation probability, it was necessary to prepare glycine supersaturated solution (S=1.7) of which 50% remained unfiltered and the other 50% was filtered using 450 nm syringe filters. Results from exposing these two batches to 1 pulse at 1064 nm are shown in figure 4.3. A drastic reduction in nucleation probability is observed for filtered samples. This concludes that NPLIN will not occur if impurities above 450 nm are absent in the sample.

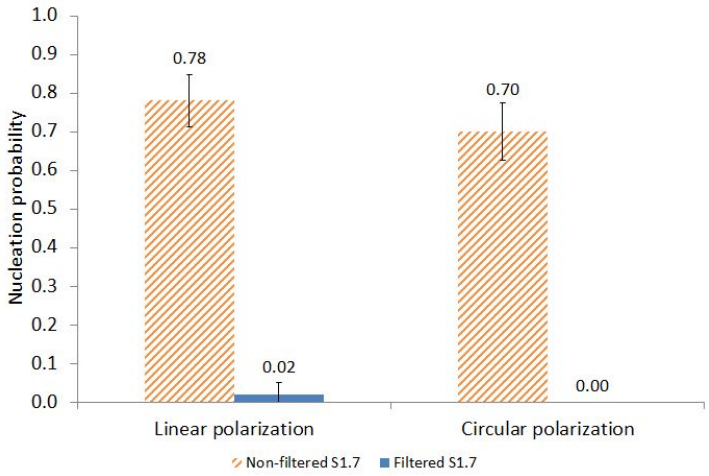

Figure 4.3: Results of filtered and non-filtered samples irradiated by 1 pulse at 1064 nm and an intensity of about 220 MW/cm^2 for solutions at supersaturation 1.7. The vials were counted 24 hours after exposure. 95% confidence intervals show the certainty of the experiments[51].

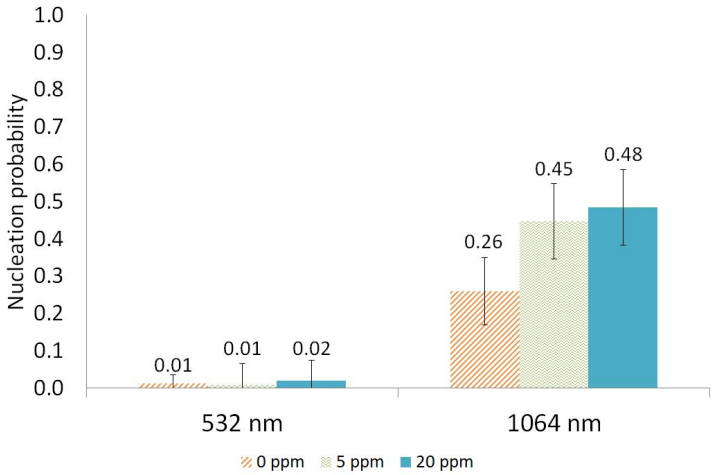

Figure 4.4: Results of iron oxide doped samples irradiated with 1 pulse linear polarized light at an intensity of 220 MW/cm^2 for glycine solution at supersaturation 1.5. Vials were counted 24 hours after exposure. 95% confidence intervals show the certainty of the experiments [51].

Impurities have so far proven to be an important factor for NPLIN behavior. However, all data is obtained at a wavelength of 1064 nm and it is not possible to generalize the outcomes due to different absorption bands at shorter wavelengths. For this reason, another set of experiments was run at 532 nm to compare the results with 1064 nm results. Both filtered and iron oxide-doped samples were exposed to a single linearly polarized pulse at 532 nm. To generalize the results to 532 nm it is important that all other parameters were kept constant. Due to the efficiency of the second harmonic crystal that converts 1064 to 532 nm, 60% of the output power is lost. The beam is then shrunk 3 times in diameter to compensate for this power loss and to maintain the same intensity (MW/cm^2). By reducing the beam size from 9 to 3 mm using 2 lens telescope, explained in section 4.2, the intensity remained 220 MW//cm^2 just as it was at 1064 nm.

The results at 532 nm are shown in figures 4.4 and 4.5. In both cases, it is clear that 532 nm has a decreasing effect on the nucleation behavior. At supersaturation 1.5, the nucleation probability dropped so much that it was unable to distinguish between doped and ”clean” samples. Therefore it is unknown if the impurity-doping process would improve the nucleation behavior at 532 nm. At higher supersaturations, there is a clear difference for filtered and non-filtered samples at both wavelengths. It becomes obvious that the nucleation probability is closely related to the availability of impurities in the sample. The reduction in probabilities at 532 nm can be explained by the reduction in the beam size and interaction volume, as is further discussed in section 4.2.

4.2. Laser interaction volume

Experiments focusing on the laser interaction volume followed immediately after the impurity experiments. After performing experiments at both of 1064 nm results to 532 nm, it was found that nucleation probabilities dropped significantly at shorter wavelengths. Former research pointed out that there was only a slight difference in probability between different wavelengths [29]. Thus, the observation was probably caused by the reduction of the beam size which subsequently also reduces the interaction volume between laser and sample. In section 3.3 no significant difference was found when using larger vials, where a larger laser interaction volume is ensured. However, these effects could have been compensated by the larger curvature of the vial which reduces the converging path of the beam and decreasing the intensity. To find out whether the laser-interaction volume is an important factor, the following hypothesis is investigated: ”Increasing the interaction volume between the laser and the sample increases the nucleation probability.”

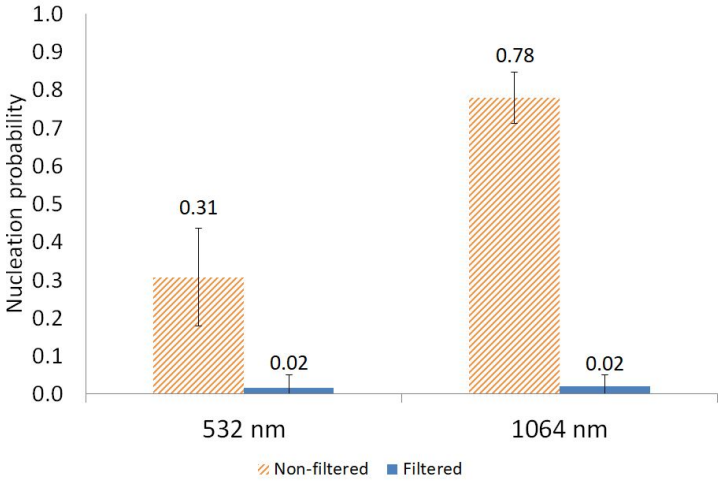

Figure 4.5: Results of filtered and non-filtered samples irradiated with 1 pulse linear polarized light at an intensity of 220 MW/cm^2 for glycine solutions at supersaturation 1.7. Vials were counted 24 hours after exposure. 95% confidence intervals show the certainty of the experiments [51].

4.2.1. Materials and methods

Samples of glycine at supersaturation 1.7 were prepared as elaborated in section 3.3. Exposure of these vials was performed slightly different, due to the unstable crystal responsible for the second harmonic generation to produce 532 nm. This crystal required a stable internal temperature to maintain a constant energy output. Because the laser was operated by shooting one pulse every ~15 seconds, this crystal started to cool down reducing the energy output. To circumvent this issue the laser was operated at continuous mode and each separate vial was exposed for 10 seconds to a train of laser pulses.

The setup for the experiments using a reduced beam size is shown in figure 4.6 and consists of the laser (532 nm), a mirror, an iris, a converging lens, a diverging lens, and the platform to support the samples. This design reduced the beam diameter from ~9 mm down to 3 mm, creating a 9 times reduction in area and a 9 times increase in the intensity. Due to the losses in the optics, 25% of the power was lost, making the intensity rise only 6.75 times. To operate all experiments at similar intensities, the second harmonic generator (crystal) was tuned accordingly. Power output was measured using a power meter (Newport 818P-030-19) to ensure similar intensities in each experiment.

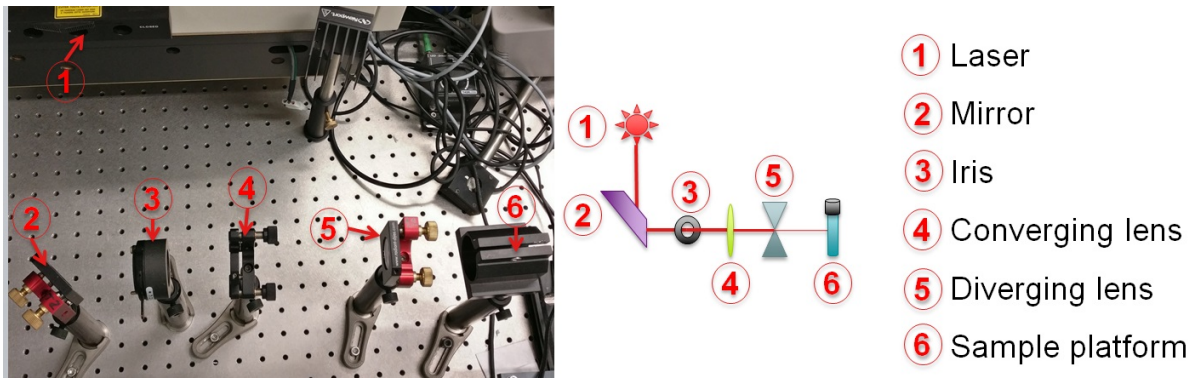

Figure 4.6: Experimental set up for reduced beam sizes.

4.2.2. Results

Several experiments were performed to investigate the dependency of the interaction volume on nucleation behavior. Little adjustments were required to obtain the setup shown in figure 4.6, including the procedure to keep as many parameters constant as possible. The final results, where only the beam diameter differs, can be found in figure 4.7. Increasing the beam size ~3 times results in a significant higher nucleation probability, about 2.5 times higher. Such a trend can be explained by homogeneous

nucleation. According to the kinetics of homogeneous nucleation, the rate scales with the volume. Increasing the interacting volume would increase the rate and thus the nucleation probability after 24 hours, as is the case in figure 4.7.

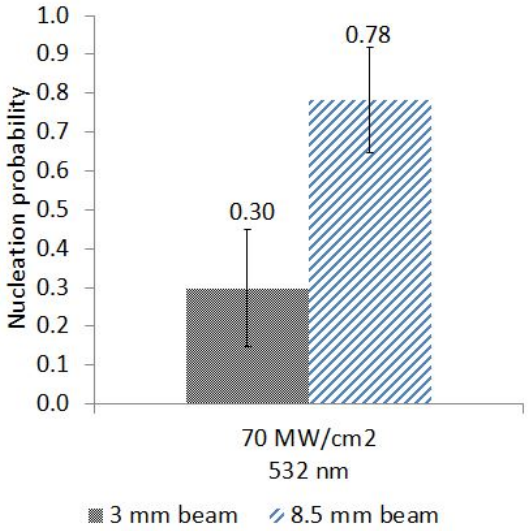

Figure 4.7: Beam diameter results of 10 seconds linear polarized irradiation and an intensity of 70 MW/cm^2 for glycine solutions at supersaturation 1.7. Vials were counted 24 hours after exposure. 95% confidence intervals show the certainty of the experiments [51].

5

Discussion, conclusion & recommendations

The purpose of present NPLIN research lies in finding the mechanism responsible for the phenomena observed in order to scale up the process to industrial size. This project aims to shed more light upon yet overlooked topics and generate more in-depth knowledge on some aspects related to laser-induced nucleation. Throughout the project, several hypotheses that required experimental and/or theoretical support have been proposed. Combining all this information will expand the knowledge base of NPLIN that is needed to scale up the process.

5.1. Discussion

Initial steps for proving non-photochemical behavior in NPLIN experimentally were made. Radicals such as hydroxyl are found to be absent in the glycine solution during laser exposure. With current equipment, it is not possible to determine whether the lack of radicals is caused by low concentrations ($\sim \mu$M) or their absence. For now, the hypothesis "the observed laser-induced nucleation in supersaturated glycine samples is non-photochemical" is accepted, based on the performed experiments and results that support the evidence described in the literature [29].

pH effects on laser-induced nucleation can be a serious factor for polymorphic control. However, in the case of glycine, this effect cannot be observed since glycine itself acts as a buffering agent. In further NPLIN research that addresses the polymorphic control requires more attention as results can be biased when batches of different pH (unknown) are used for other experimental setups.

When using glycine, special attention must be attributed to the coloration of the samples, especially when vials are exposed to wavelengths below 500 nm where a higher absorbance is expected. Such energy absorbance increases the temperature of the vial which results in a decrease of the supersaturation that eventually reduces the nucleation likelihood [27]. At longer wavelengths, the nucleation probability is less likely to be affected, as the formation of NH_4^+ (and thus the reduction of glycine) is negligible, orders of ppm. It is recommended to use the glycine samples not longer than 4 months to keep a high level of consistency during experiments.

The glassware experiments together with the beam size experiments showed clearly that the exposed volume is of utmost importance to maintain a high nucleation probability. Small circular vials with a diameter of 1.6 cm act as a focusing cylindrical lens increasing the laser intensity. Experiments with larger circular vials, 2.2 cm in diameter, showed similar nucleation probability, despite having less self-focusing capabilities which would lower the intensity. The square vials, 2.6 cm in width, do not self-focus the beam at all but ensure the same nucleation probability by a large laser interaction volume. The beam size experiments verified this volume interaction dependency for nucleation probabilities.

Another insight gained from the glassware experiments is the effect of the curvature on the laser-solution interaction. Initially, it was thought that polymorphic control was performed by adjusting the polarization [9]. Several experiments indicated that this polarization switching was non-existent [3, 27]. During the experiments in this project, it was observed that polymorphic control seems to be affected by the surface curvature. Generally, circular polarization could become slightly more elliptical when using circular vials, affecting polymorphic outcomes. Minor differences in vial diameter would result in different polarization properties, thus explaining the contradictory results reported in the literature. The mentioned hypothesis: "Glycine polymorphism is dependent on the polarization switching for both flat and circular geometries" is accepted partially with current knowledge. It was found to be true for flat surfaces, however, it did not hold for curved surfaces. For deeper research into polymorphic control, it is recommended to use vials with flat surfaces and have a square cross-section.

NPLIN is known to be affected by impurities present in the solution. As discussed in chapter 3 this effect becomes more apparent at higher supersaturations (1.7). The removal of impurities made the nucleation probability to drop to nearly zero. On the other hand, when intentionally doping the samples with known amounts of impurities, was slightly increasing the probability. The observed phenomena hold for linear polarization, but not as much for circular polarization.

5.2. Conclusion

To conclude this project, glycine was found to be susceptible to NPLIN depending on several parameters such as laser interaction volume, impurities, and glass shapes. Under current conditions, the nucleation process is still claimed to be non-photochemical. More research is required to prove this. An experimental setup for further investigation into the radical formation is developed.

Factors affecting the way glycine behaves in solutions are acknowledged and tracked to maintain the sample as stable as possible. The glycine discoloration and pH are found to be irrelevant during the NPLIN experiments. However, special care is required for future research when new chemicals are tested. Furthermore, glass container shapes affect the polymorphic output significantly during laser-induced nucleation.

Impurities were the last factor being checked. The nucleation probability is improved adding impurities and significantly reduced when removing the impurities. Current in-house research suspects that the nucleation is triggered by the existence of a cavitation bubble, caused by impurities absorbing energy from the laser beam. More evidence is gathered to support the NPLIN phenomena in terms of the external variables as explained in subsection 1.3.2.

5.3. Recommendations

Unfortunately, as all things come to an end, this project finished in April 2019. Since a lot of topics require deeper investigation, the following points are raised for the continuation of the NPLIN research.

- *Further exploration of radical measurements:* to conclude that the hydroxyl radical is not formed during NPLIN, more experiments are required. To detect fluorescence at very low concentrations a new and more sensitive spectrometer needs to be acquired. Also, the lower threshold concentration of the dye has to be determined to ensure non-photochemical effects in laser-induced nucleation. Another important point would be the use of the FTIR that is already available. Researchers found IR spectra of relevant glycine radicals that can be measured using an FTIR [52];
- *Exposure of increased volumes:* this research pointed out that an increased laser interaction volume provides enhanced nucleation probabilities. This is good for scaling up the process, as it becomes more efficient at a larger scale. The volume effect needs verification for significant bigger containers, e.g. liters instead of ml;
- *Micro-impurity behavior:* current statements regarding the impurity doping mainly apply to the nano-regime. To generalize, experiments with micro-scale impurities need to be carried as impurities above 450 nm showed to be an important promoter to NPLIN;

- *Polymorphic control on other compounds:* the polarization window raised by Sun et al. is still not fully eliminated as a topic. Research into polymorphic control must be done more carefully by keeping the pH constant and using flat laser interaction surfaces; that would be specifically effective when looking into new NPLIN-chemicals.

A

Time terminology

In the early stages of the project it was unclear what part of the sample preparation period was meant when using particular terminology. The graph below serves as a visual overview of all terms used during the research. Waiting time is often referred to as ”aging”.

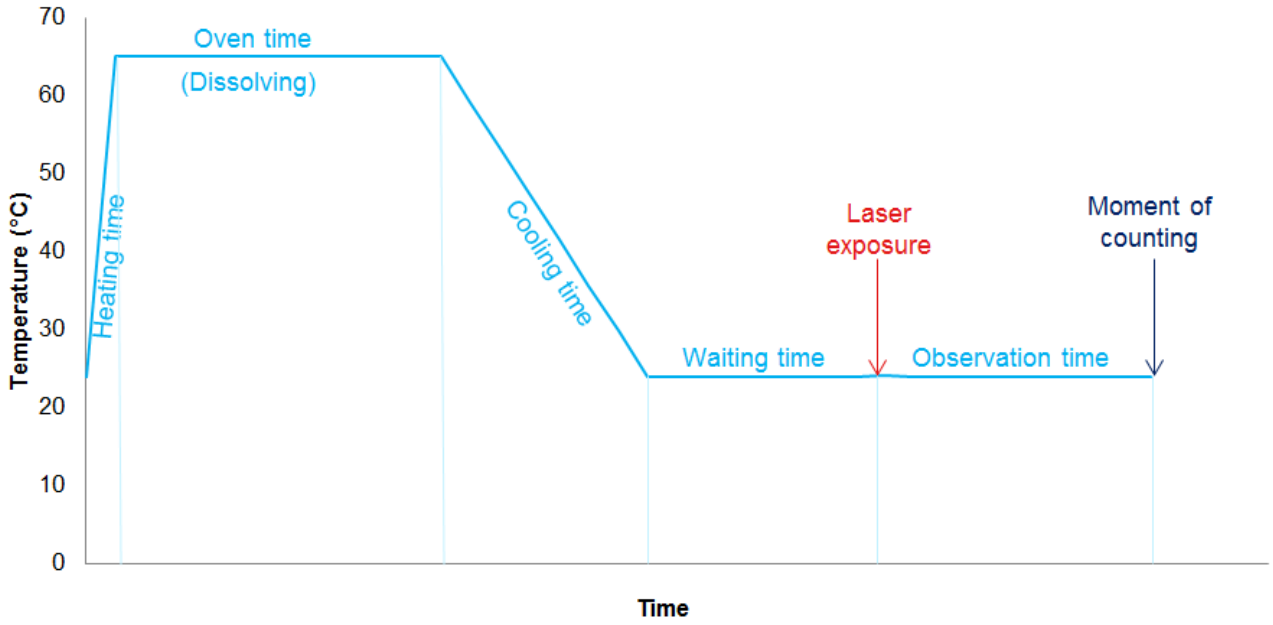

Figure A.1: Schematic representation of the standard sample handling stages and the corresponding terminology to prevent confusion.

B

Summarized NPLIN results

A summary was made of all experiments performed. All convenient parameters for all these experiments is shown in figure B.1.

Date of exposure =	Supersaturation =	Polarization =	Wavelength =	Power =	Aging =	Containing other particles =	Concentration other partic. =	Am. of pulses =	Glass type =	Volume vials =	pH before vials =	Nucl. Probability	CI	Gam. Probability	CI
25-9-2018	1.6	Linear	1064	10	0	none	none	1	Circular	8	unknown	18%	0.08		
8-10-2018	1.6	Linear	1064	10	0	none	none	1	Circular	8	unknown	22%	0.09		
8-10-2018	1.5	Linear	1064	10	2	none	none	1	Circular	8	5.5	29%	0.09		
16-10-2018	1.6	Linear	1064	10	0	none	none	1	Circular	8	unknown	15%	0.08		
22-10-2018	1.5	Linear	1064	10	0	none	none	1	Circular	8	5.5	6%	0.05		
31-10-2018	1.5	Linear	1064	10	0	none	none	1	Circular	8	5.5	4%	0.04	50%	0.01
5-11-2018	1.5	Linear	1064	10	2	none	none	1	Circular	8	5.5	6%	0.04	0%	0.00
12-11-2018	1.7	Linear	1064	10	2	none	none	1	Circular	8	5.67	79%	0.09	40%	0.10
15-11-2018	1.5	Linear	1064	10	2	none	none	1	Circular	8	5.65	26%	0.09	9%	0.02
19-11-2018	1.5	Linear	1064	10	2	silica	5	1	Circular	8	5.65	29%	0.10	6%	0.03
26-11-2018	1.5	Circular	1064	10	2	none	none	1	Circular	8	5.65	14%	0.08	8%	0.02
26-11-2018	1.5	Circular	1064	10	2	Silica	5	1	Circular	8	5.65	17%	0.09	9%	0.03
30-11-2018	1.7	Linear	1064	10	2	none	none	600	Circular	8	5.45	90%	0.07	85%	0.08
10-12-2018	1.7	Circular	1064	10	2	none	none	1	Circular	8	5.45	42%	0.12	33%	0.08
13-12-2018	1.5	Linear	1064	10	2	none	none	1	Square	15	5.44	20%	0.08	78%	0.04
17-12-2018	1.7	Linear	1064	10	2	none	none	1	Circular	8	unknown	97%	0.04	99%	0.00
17-12-2018	1.5	Linear	1064	10	2	none	none	1	Circular	8	unknown	6%	0.06	50%	0.03
17-12-2018	1.6	Linear	1064	10	2	none	none	1	Circular	8	unknown	20%	0.10	100%	0.00
20-12-2018	1.5	Linear	1064	10	2	none	none	1	Circular	15	5.44	9%	0.06	56%	0.03
20-12-2018	1.5	Linear	1064	10	2	Silica	100	1	Circular	8	Unknown	34%	0.10	94%	0.03
10-1-2019	1.5	Circular	1064	10	2	none	none	1	Square	15	5.44	8%	0.06	29%	0.03
14-1-2019	1.5	Circular	1064	10	2	Silica	100	1	Circular	8	Unknown	8%	0.06	0%	0.00
14-1-2019	1.5	Linear	1064	10	2	none	none	1	Circular	8	Unknown	5%	0.06	67%	0.03
14-1-2019	1.7	Circular	1064	10	2	none	none	600	Circular	8	5.45	86%	0.08	47%	0.10
14-1-2019	1.6	Linear	1064	10	2	none	none	1	Circular	8	Unknown	5%	0.06	0%	0.00
17-1-2019	1.5	Circular	1064	10	2	none	none	1	Circular	15	5.44	6%	0.05	50%	0.02
17-1-2019	1.7	Circular	1064	10	1.5	none	none	1	Circular	8	Unknown	98%	0.03	100%	0.00
21-1-2019	1.5	Linear	1064	10	2	Iron oxide	20	1	Circular	8	5.32	48%	0.10	2%	0.02
21-1-2019	1.5	Linear	1064	10	2	Iron oxide	5	1	Circular	8	5.3	45%	0.10	14%	0.05
23-1-2019	1.5	Linear	1064	10	0	none	none	1	Circular	8	unknown	8%	0.07	70%	0.03
23-1-2019	1.6	Linear	1064	10	0	none	none	1	Circular	8	unknown	8%	0.07	100%	0.00
4-2-2019	1.6	Linear	1064	10	4	none	none	1	Circular	8	unknown	4%	0.05	100%	0.00
4-2-2019	1.7	Linear	1064	10	2	none	none	1	Circular	8	unknown	99%	0.03	100%	0.00
4-2-2019	1.6	Circular	1064	10	2	Iron oxide	5	1	Circular	8	5.3	20%	0.08	16%	0.03
11-2-2019	1.7	Linear	1064	10	2	none	none	1	Circular	8	unknown	34%	0.11	69%	0.07
11-2-2019	1.7	Linear	1064	10	2	Filtered 0.45 µm	Filtered 0.45 µm	1	Circular	8	unknown	2%	0.03	0%	0.00
12-2-2019	1.7	Linear	1064	10	3	Filtered 0.45 µm	Filtered 0.45 µm	1	Circular	8	unknown	0%	0.00	0%	0.00
14-2-2019	1.5	Circular	1064	10	1.5	Iron oxide	20	1	Circular	8	unknown	9%	0.06	0%	0.00
14-2-2019	1.7	Circular	1064	10	2	none	none	1	Circular	8	unknown	30%	0.10	48%	0.06
21-2-2019	1.7	Circular	1064	10	2	Filtered 0.45 µm	Filtered 0.45 µm	1	Circular	8	unknown	9%	0.07	20%	0.03
21-2-2019	1.5	Linear	1064	10	2	Silica	100	1	Circular	8	unknown	2%	0.03	0%	0.00
28-2-2019	1.5	Linear	532	3.2	2	Iron oxide	5	1	Circular	8	unknown	9%	0.06	25%	0.03
28-2-2019	1.5	Linear	532	3.2	2	Iron oxide	20	1	Circular	8	unknown	9%	0.06	0%	0.00
11-3-2019	1.7	Linear	532	1.4	2	Filtered 0.45 µm	Filtered 0.45 µm	1	Circular	8	unknown	2%	0.03	0%	0.00
11-3-2019	1.7	Linear	532	1.4	2	none	none	1	Circular	8	unknown	31%	0.13	63%	0.07
11-3-2019	1.5	Linear	532	1.4	2	none	none	1	Circular	8	unknown	1%	0.02	0%	0.00
18-3-2019	1.7	Linear	532	3.2	3	none	none	1	Circular	8	Unknown	25%	0.15	88%	0.06
18-3-2019	1.7	Linear	532	0.5	3	none	none	1	Circular	8	Unknown	16%	0.12	100%	0.00
21-3-2019	1.5	Linear	532	1.4	2	Iron oxide	5	1	Circular	8	Unknown	1%	0.02	0%	0.00
21-3-2019	1.5	Linear	532	1.4	2	Iron oxide	20	1	Circular	8	Unknown	2%	0.03	0%	0.00
25-3-2019	1.7	Linear	1064	10	2	none	none	1	Circular	8	Unknown	66%	0.12	58%	0.10

Figure B.1: A summary of all performed experiments that focused on probabilities or polymorphism. CI = 95% Confidence Interval

C

Particle size distributions

During the research use was made of the malvern zetasizer, a device that measures particle size distributions based on diffusivity of particular components. A picture is made each timespan. By tracking molecules from one snapshot to another a certain speed can be derived. Using this speed together with the known temperature and viscosity of the sample provides a diffusivity that can be related to the particle size. This method initially mentions the intensity distribution as this is measured quantity. From the intensity distribution it is possible to derive a volume distribution, see equation C.1 by assuming a perfect sphere and number distribution with equation C.2 estimating the numbers using the Mie theory, where I is the intensity, N the number and M the Mie factor at x.

$$V(x) = \frac{4}{3}\pi(\frac{x}{2})^3 \tag{C.1}$$

$$I(x) = N(x)M(x,_{D,P}) \tag{C.2}$$

Three different intensity based particle size distributions can be found below. Each graph is related to a topic discussed in section 4.1 and serves as fundamental for containing the expected particles. A reoccurring peak is observed at 1 nm. This peak is likely to be attributed to small monomers of glycine, as the size of a single glycine molecule is estimated to be 0.42 nm [53].

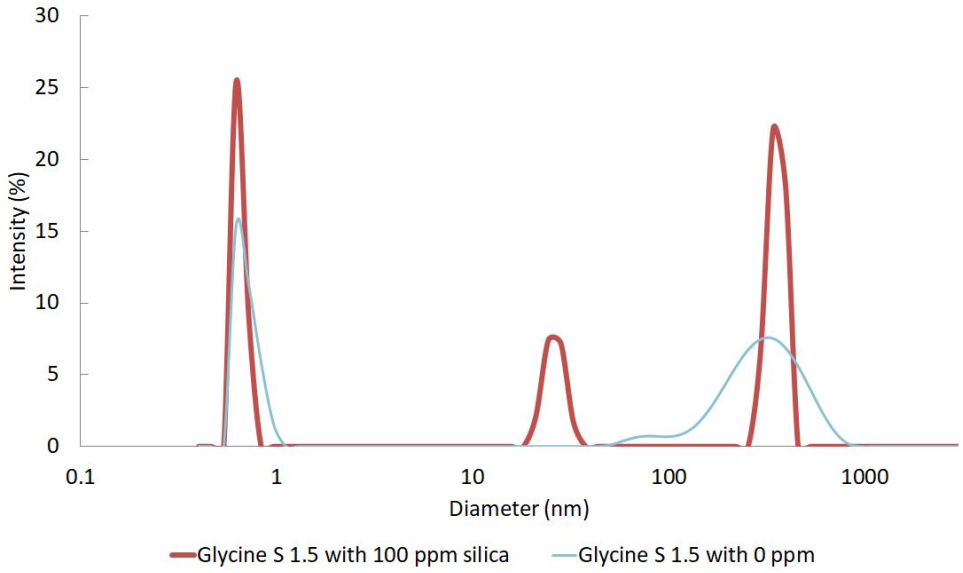

Figure C.1: Intensity based particle size distribution for the 0 and 100 ppm silica doped glycine solution. Both solutions were diluted 2 times in order to prevent spontaneous nucleation at room temperature.

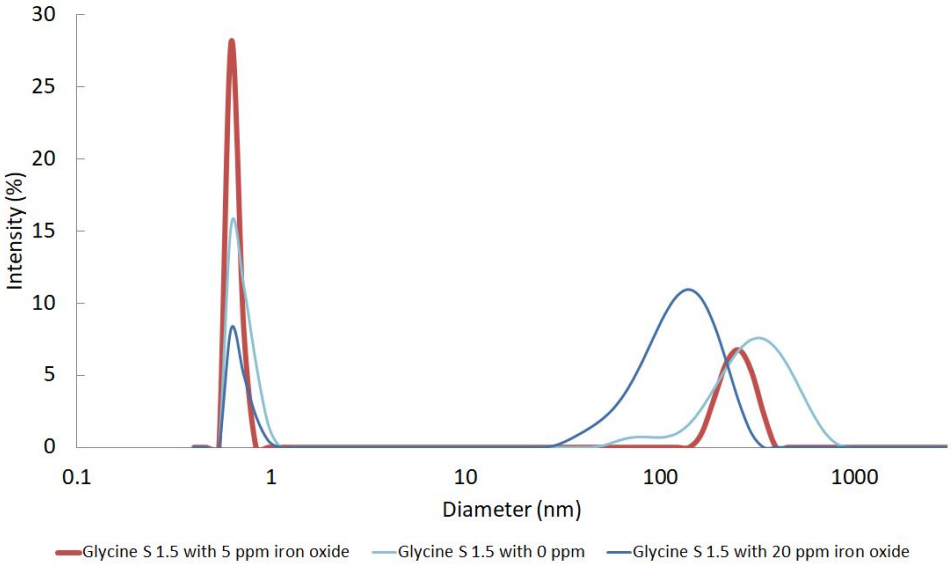

Figure C.2: Intensity based particle size distribution for the 0, 5 and 20 ppm iron oxide doped glycine solution. All solutions were diluted 2 times in order to prevent spontaneous nucleation at room temperature.

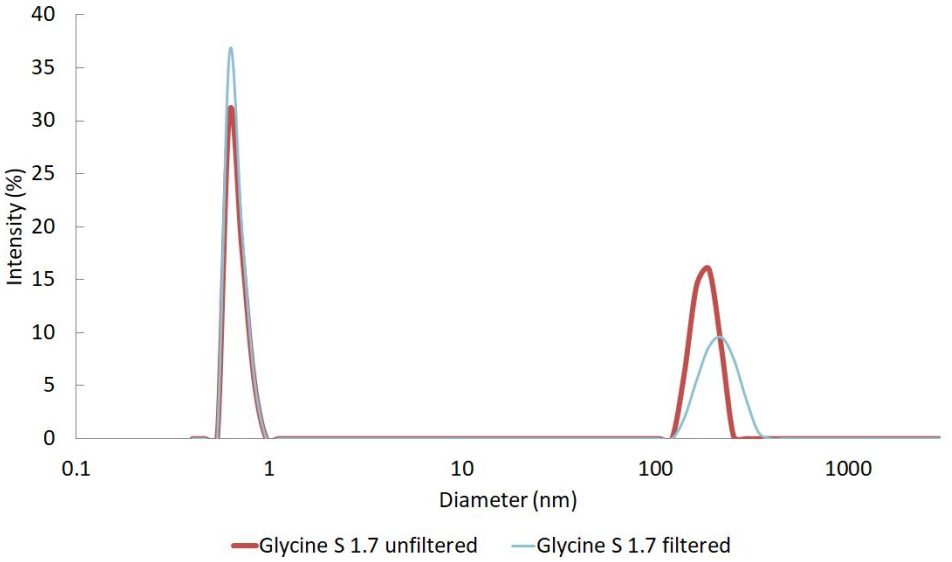

Figure C.3: Intensity based particle size distribution for the filtered and unfiltered glycine supersaturation 1.7 solutions. All solutions were diluted 2 times in order to prevent spontaneous nucleation at room temperature. The graph clearly shows a shift in peak size at sizes larger than 450 nm, the point where all impurities were removed.

D

Ultraviolet visible spectroscopy results

Two extra graphs of UV-vis measurements are provided below, supporting the experiments discussed in section 4.1.

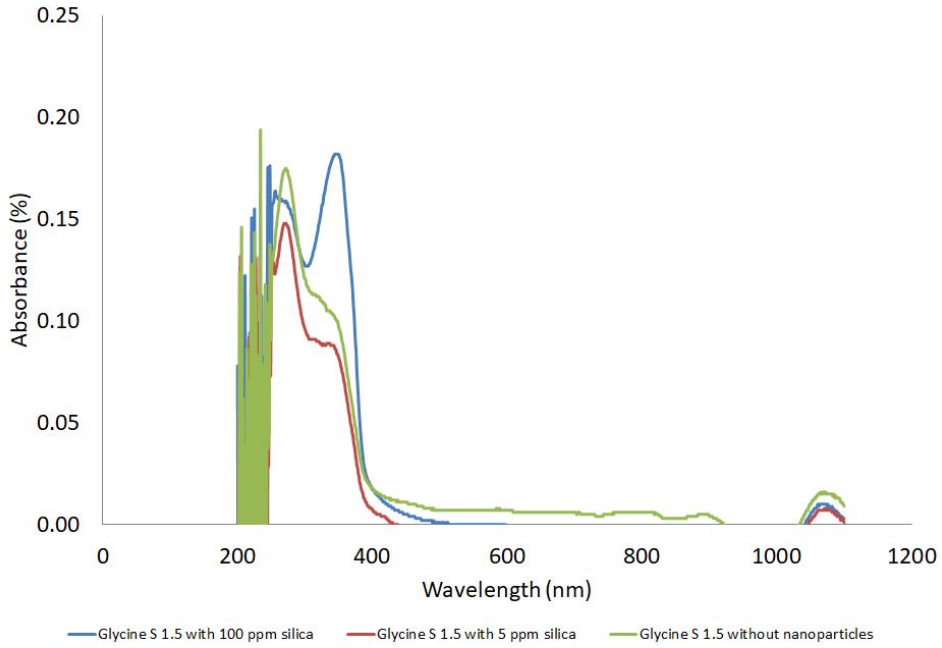

Figure D.1: UV-vis absorbance spectrum for silica doped glycine solutions. Measurements below 250 nm become inaccurate due to absorption of light by the cuvette. A small valley is found around 1000 nm which is caused by the reference sample containing 100% water.

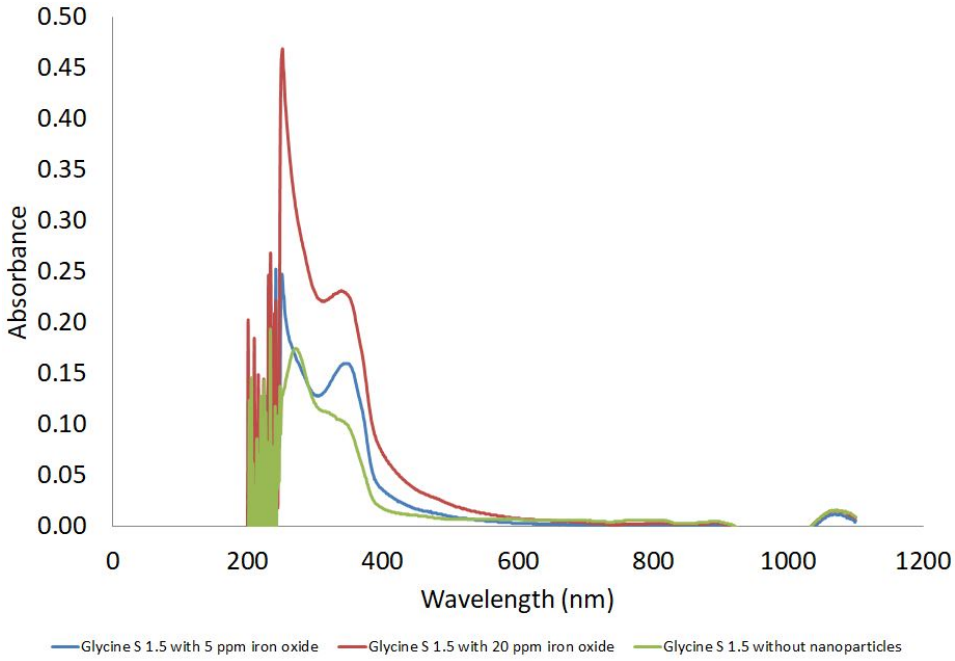

Figure D.2: UV-vis absorbance spectrum for iron oxide doped glycine solutions. Measurements below 250 nm become inaccurate due to absorption of light by the cuvette. A small valley is found around 1000 nm which is caused by the reference sample containing 100% water.

Bibliography

[1] B. A. Garetz, J. E. Aber, N. L. Goddard, R. G. Young, and A. S. Myerson, *Nonphotochemical, polarization-dependent, laser-induced nucleation in supersaturated aqueous urea solutions,* Physical Review Letters **77**, 3475 (1996).

[2] J. E. Aber, S. Arnold, B. A. Garetz, and A. S. Myerson, *Strong dc electric field applied to supersaturated aqueous glycine solution induces nucleation of the γ polymorph,* Physical Review Letters **94**, 1 (2005).

[3] Y. Liu, M. H. Van Den Berg, and A. J. Alexander, *Supersaturation dependence of glycine polymorphism using laser-induced nucleation, sonocrystallization and nucleation by mechanical shock,* Physical Chemistry Chemical Physics **19**, 19386 (2017).

[4] N. Radacsi, J. H. Ter Horst, and G. D. Stefanidis, *Microwave-assisted evaporative crystallization of niflumic acid for particle size reduction,* Crystal Growth and Design **13**, 4186 (2013).

[5] D. Erdemir, A. Y. Lee, and A. S. Myerson, *Nucleation of crystals from solution: classical and two-step models,* Accounts of Chemical Research **42**, 621 (2009).

[6] J. Mullin, *Butterworth-Heinemann*, Vol. 4 (2001) pp. 1–610.

[7] J. Zaccaro, J. Matic, A. S. Myerson, and B. A. Garetz, *Nonphotochemical, laser-induced nucleation of supersaturated aqueous glycine produces unexpected γ-polymorph,* Crystal Growth and Design **1**, 5 (2001).

[8] A. Llinàs and J. M. Goodman, *Polymorph control: past, present and future,* Drug Discovery Today **13**, 198 (2008).

[9] X. Sun, B. a. Garetz, and A. S. Myerson, *Supersaturation and Polarization Dependence of Polymorph Control in the Nonphotochemical Laser-Induced Nucleation (NPLIN) of Aqueous Glycine Solutions,* Crystal Growth & Design **6**, 684 (2006).

[10] A. Ikni, B. Clair, P. Scouflaire, S. Veesler, J. M. Gillet, N. El Hassan, F. Dumas, and A. Spasojević-De Biré, *Experimental demonstration of the carbamazepine crystallization from non-photochemical laser-induced nucleation in acetonitrile and methanol,* Crystal Growth and Design **14**, 3286 (2014).

[11] X. Sun, B. A. Garetz, and A. S. Myerson, *Polarization switching of crystal structure in the nonphotochemical laser-induced nucleation of supersaturated aqueous l-histidine,* Crystal Growth and Design **8**, 1720 (2008).

[12] Y. Liu, M. R. Ward, and A. J. Alexander, *Polarization independence of laser-induced nucleation in supersaturated aqueous urea solutions,* Physical Chemistry Chemical Physics **19**, 3464 (2017).

[13] A. J. Alexander and P. J. Camp, *Single Pulse, Single Crystal Laser-Induced Nucleation of Potassium Chloride,* Crystal Growth & Design **9**, 958 (2009).

[14] M. R. Ward, A. M. Mackenzie, and A. J. Alexander, *Role of Impurity Nanoparticles in Laser-Induced Nucleation of Ammonium Chloride,* Crystal Growth and Design **16**, 6790 (2016).

[15] M. R. Ward, I. Ballingall, M. L. Costen, K. G. McKendrick, and A. J. Alexander, *Nanosecond pulse width dependence of nonphotochemical laser-induced nucleation of potassium chloride,* Chemical Physics Letters **481**, 25 (2009).

[16] M. R. Ward, W. J. Jamieson, C. A. Leckey, and A. J. Alexander, *Laser-induced nucleation of carbon dioxide bubbles,* Journal of Chemical Physics **142** (2015), 10.1063/1.4917022.

[17] J. O. Sindt, A. J. Alexander, and P. J. Camp, *Effects of nanoparticle heating on the structure of a concentrated aqueous salt solution,* Journal of Chemical Physics **147** (2017), 10.1063/1.5002002.

[18] M. R. Ward, A. Rae, and A. J. Alexander, *Nonphotochemical Laser-Induced Crystal Nucleation by an Evanescent Wave,* Crystal Growth and Design **15**, 4600 (2015).

[19] M. R. Ward, S. McHugh, and A. J. Alexander, *Non-photochemical laser-induced nucleation of supercooled glacial acetic acid,* Physical Chemistry Chemical Physics **14**, 90 (2012).

[20] A. J. Alexander and P. J. Camp, *Non-photochemical laser-induced nucleation,* Journal of Chemical Physics **150** (2019), 10.1063/1.5079328.

[21] B. A. Garetz, J. Matic, and A. S. Myerson, *Polarization Switching of Crystal Structure in the Non-photochemical Light-Induced Nucleation of Supersaturated Aqueous Glycine Solutions,* Physical Review Letters **89**, 1 (2002).

[22] J. Matic, X. Sun, B. A. Garetz, and A. S. Myerson, *Intensity, wavelength, and polarization dependence of nonphotochemical laser-induced nucleation in supersaturated aqueous urea solutions,* Crystal Growth and Design **5**, 1565 (2005).

[23] K. Fang, S. Arnold, and B. A. Garetz, *Nonphotochemical laser-induced nucleation in levitated supersaturated aqueous potassium chloride microdroplets,* Crystal Growth and Design **14**, 2685 (2014).

[24] I. S. Lee, J. M. B. Evans, D. Erdemir, A. Y. Lee, B. A. Garetz, and A. S. Myerson, *Nonphotochemical Laser Induced Nucleation of Hen Egg White Lysozyme Crystals,* Crystal Growth & Design **8**, 4255 (2008).

[25] R. Kacker, S. Dhingra, D. Irimia, M. K. Ghatkesar, A. Stankiewicz, H. J. Kramer, and H. B. Eral, *Multiparameter Investigation of Laser-Induced Nucleation of Supersaturated Aqueous KCl Solutions,* Crystal Growth and Design **18**, 312 (2018).

[26] R. J. E. Meijers, *The Effect of Impurities and Light Polarization on NPLIN The Effect of Impurities and Light Polarization on NPLIN By*, Ph.D. thesis, TU Delft (2018).

[27] A. S. Garg, *Investigating possible mechanisms of Non- Photochemical Laser Induced Nucleation*, Ph.D. thesis, TU Delft (2018).

[28] S. Dhingra, *Understanding Non-Photochemical Laser Induced Nucleation*, Ph.D. thesis, TU Delft (2017).

[29] B. C. Knott, J. L. Larue, A. M. Wodtke, M. F. Doherty, and B. Peters, *Communication: Bubbles, crystals, and laser-induced nucleation,* Journal of Chemical Physics **134** (2011), 10.1063/1.3582897.

[30] E. W. van Stryland, D. R. Williams, and W. L. Wolfe, *Handbook of optics: devices, measurements, & properties*, 2nd ed., edited by M. Bass (McGRAW-HILL, Inc., New York, 1995) p. 1496.

[31] N. Mirsaleh-Kohan, A. Fischer, B. Graves, M. Bolorizadeh, D. Kondepudi, and R. N. Compton, *Laser shock wave induced crystallization,* Crystal Growth and Design **17**, 576 (2017).

[32] W. Christian and M. Belloni, *Capacitance and Dielectrics,* in *Physlet Physics* (2013) 3rd ed.

[33] C. Duffus, P. J. Camp, and A. J. Alexander, *Spatial control of crystal nucleation in agarose gel,* Journal of the American Chemical Society **131**, 11676 (2009).

[34] N. Estime, S. Teychené, J.-M. Autret, and B. Biscans, *Influence of pH, Temperature and Impurities on the Solubility of an Active Pharmaceutical Ingredient (API),* International Journal of Chemical Reactor Engineering **8** (2010), 10.2202/1542-6580.2099.

[35] R. Carta and G. Tola, *Solubilities of l -Cystine, l -Tyrosine, l-Leucine, and Glycine in Aqueous Solutions at Various pHs and NaCl Concentrations,* Journal of Chemical & Engineering Data **41**, 414 (1996).

[36] T. Uwada, S. Fujii, T. Sugiyama, A. Usman, A. Miura, H. Masuhara, K. Kanaizuka, and M. A. Haga, *Glycine crystallization in solution by CW laser-induced microbubble on gold thin film surface,* ACS Applied Materials and Interfaces **4**, 1158 (2012).

[37] M. Bonifačić, I. Štefanić, G. L. Hug, D. A. Armstrong, and K. D. Asmus, *Glycine decarboxylation: The free radical mechanism,* Journal of the American Chemical Society **120**, 9930 (1998).

[38] P. Berger, N. K. vel Leitner, M. Dore, and B. Legube, *Ozone and hydroxyl radicals induced oxidation of glycine,* Wat. Res. **33**, 433 (1998).

[39] T. Okutsu, K. Nakamura, H. Haneda, and H. Hiratsuka, *Laser-Induced Crystal Growth and Morphology Control of Benzopinacol Produced from Benzophenone in Ethanol/Water Mixed Solution,* Crystal Growth and Design **4**, 113 (2004).

[40] T. Okutsu, K. Isomura, N. Kakinuma, H. Horiuchi, M. Unno, H. Matsumoto, and H. Hiratsuka, *Laser-induced morphology control and epitaxy of dipara-anthracene produced from the photochemical reaction of anthracene,* Crystal Growth and Design **5**, 461 (2005).

[41] J. C. Mierzwa, R. Rodrigues, and A. C. Teixeira, *Advanced Oxidation Processes for Wastewater Treatment: Emerging Green Chemical Technology* (2018) pp. 13–48.

[42] N. Javid, T. Kendall, I. S. Burns, and J. Sefcik, *Filtration suppresses laser-induced nucleation of glycine in aqueous solutions,* Crystal Growth and Design **16**, 4196 (2016).

[43] B. N. Moolya, A. Jayarama, M. R. Sureshkumar, and S. M. Dharmaprakash, *Hydrogen bonded nonlinear optical γ-glycine: Crystal growth and characterization,* Journal of Crystal Growth **280**, 581 (2005).

[44] I. M. Weiss, C. Muth, R. Drumm, and H. O. Kirchner, *Thermal decomposition of the amino acids glycine, cysteine, aspartic acid, asparagine, glutamic acid, glutamine, arginine and histidine,* BMC Biophysics **11**, 1 (2018).

[45] C. C. Loures, M. A. K. Alcântara, H. J. Izario Filho, A. C. S. C. Teixeira, F. T. Silva, T. C. B. Paiva, and G. R. L. Samanamud, *Advanced Oxidative Degradation Processes: Fundamentals and Applications,* International Review of Chemical Engineering **5**, 102 (2013).

[46] W. Li, A. Ikni, P. Scouflaire, X. Shi, N. El Hassan, P. Gémeiner, J. M. Gillet, and A. Spasojević-De Biré, *Non-Photochemical Laser-Induced Nucleation of Sulfathiazole in a Water/Ethanol Mixture,* Crystal Growth and Design **16**, 2514 (2016).

[47] X. Yang, X. Wang, and C. B. Ching, *Solubility of form α and form γ of glycine in aqueous solutions,* Journal of Chemical and Engineering Data **53**, 1133 (2008).

[48] M. N. Bhat and S. M. Dharmaprakash, *Growth of nonlinear optical γ-glycine crystals,* Journal of Crystal Growth **236**, 376 (2002).

[49] X. Yang, C. Ching, X. Wang, and J. Lu, *Polymorphism in the crystallization of glycine,* AICHE annual meeting, San … (2006).

[50] E. Seyedhosseini, M. Ivanov, V. Bystrov, I. Bdikin, P. Zelenovskiy, V. Y. Shur, A. Kudryavtsev, E. D. Mishina, A. S. Sigov, and A. L. Kholkin, *Growth and nonlinear optical properties of β-glycine crystals grown on pt substrates,* Crystal Growth and Design **14**, 2831 (2014).

[51] G. Cumming, F. Fidler, and D. L. Vaux, *Error bars in experimental biology,* Journal of Cell Biology **177**, 7 (2007), arXiv:Error bars in experimental biology .

[52] B. Minaev and O. Lut, *Calculation of structure and spectra of the glycine radical with dehydrogenated carboxyl group,* Ukrainica Bioorganica … **2**, 35 (2009).

[53] C. Poole and O. F. J, *Introduction to Nanotechnology,* Wiley , 311 (2003).